Tracing Biosignature Preservation of Geothermally Silicified Microbial Textures into the Geological Record

Kathleen A. Campbell,[1] Bridget Y. Lynne,[2] Kim M. Handley,[3,4] Sacha Jordan,[4] Jack D. Farmer,[5] Diego M. Guido,[7] Frédéric Foucher,[8] Susan Turner,[9] and Randall S. Perry[10]

Abstract

New Zealand and Argentine (Late Jurassic–Recent) siliceous hot-spring deposits (sinter) reveal preservation pathways of environmentally controlled, microbe-dominated sedimentary facies over geological time scales. Texturally distinctive, laminated to thinly layered, dense and vertically oriented, microtubular "palisade" fabric is common in low-temperature ($<40°C$) sinter-apron terraces. In modern hot springs, the dark green to brown, sheathed, photosynthetic cyanobacterium *Calothrix* spp. (family Rivulariaceae) constructs felted palisade mats in shallow terrace(tte) pools actively accreting opaline silica. The resulting stacked layers of silicified coarse filaments—a stromatolite—are highly porous and readily modified by postdepositional environmental perturbations, secondary silica infill, and diagenetic silica phase mineral transformations (opal-A to quartz). Fossil preservation quality is affected by relative timing of silicification, and later environmental and geological events.

A systematic approach was used to characterize palisade fabric in sinters of different ages to refine tools for recognizing biosignatures in extreme environments and to track their long-term preservation pathways into the geological record. Molecular techniques, scanning electron microscopy, Raman spectrometry, X-ray powder diffraction, petrography, and lipid biomarker analyses were applied. Results indicate that microbial communities vary at the micron scale and that early and rapid silicification is paramount to long-term preservation, especially where minimal postdepositional disturbance follows fossilization. Overall, it appears that the most robust biomarkers of fossil microbial activity in hot-spring deposits are their characteristic macro- and microtextures and laser micro-Raman identified carbon. Studies of Phanerozoic geothermal deposits with mineralized microbial components are relevant analogs for Precambrian geobiology because early life is commonly preserved as microbial microfossils and biofilms in silica, some of it hydrothermal in origin. Yet the diagenetic "movie" has already been run. Hence, studying younger sinters of a range of ages provides an opportunity to "play it again" and follow the varied influences on biosignatures into the deep-time geological record. Key Words: Hot springs—Diagenesis—Silica—Microbial mats—Fossilization. Astrobiology 15, 858–882.

1. Introduction

SINTERS ARE continental hot-spring deposits that largely form in volcanic terrains where near-neutral, alkali-chloride, silica-rich fluids, derived from magmatically heated reservoirs ($>175°C$), ascend rapidly to the surface to discharge in geysers and hot springs (Renaut and Jones, 2011).

The silica carried in solution nucleates, polymerizes, and precipitates upon surfaces in evaporatively cooling thermal pools and discharge channels (Fournier and Rowe, 1966; Weres and Apps, 1982; Fournier, 1985; Williams and Crerar, 1985). Geothermally associated prokaryotes and eukaryotes (*e.g.*, thermophilic microbes, plants, insects, diatoms) become mineralized into mound buildups and terraced sinter

[1]Earth Science Programme, School of Environment, The University of Auckland, Auckland, New Zealand.
[2]Department of Engineering Science, The University of Auckland, Auckland, New Zealand.
[3]Department of Ecology and Evolution, The University of Chicago, Chicago, Illinois, USA.
[4]School of Biological Sciences, The University of Auckland, Auckland, New Zealand.
[5]School of Earth and Space Exploration, Arizona State University, Tempe, Arizona, USA.
[7]CONICET-UNLP, Instituto de Recursos Minerales, La Plata, Argentina.
[8]Exobiology Research Group, Centre de Biophysique Moléculaire, CNRS, Orléans, France.
[9]BioConsortia, Inc., Davis, California, USA.
[10]Impacts and Astromaterials Research Centre, Earth Sciences and Engineering, Imperial College London, South Kensington Campus, London, UK.
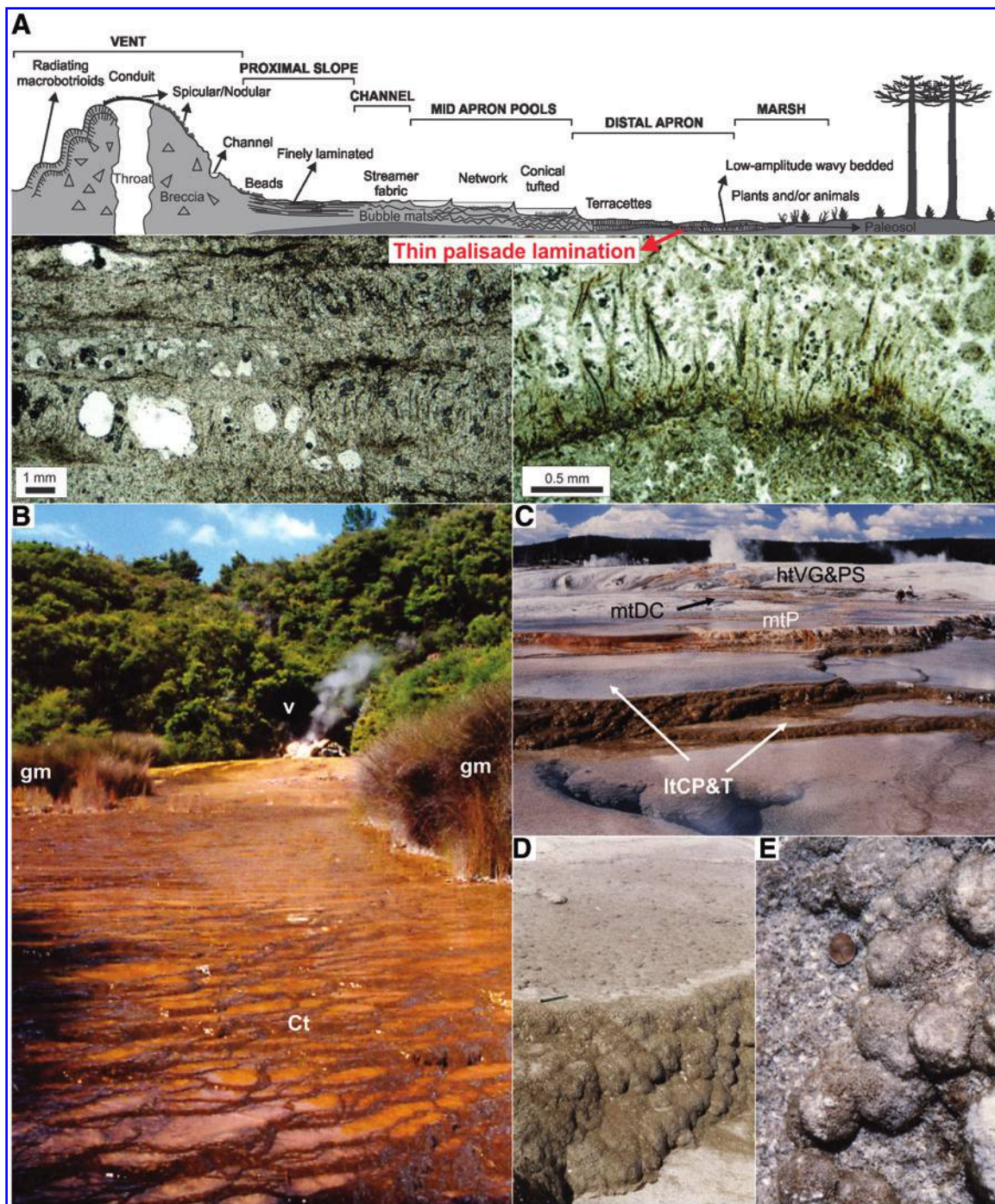
FIG. 1. Environmental setting of low-temperature (<40°C) palisade sinter in a siliceous hot-spring environmental gradient from vent (∼100°C) to geothermally influenced marsh facies (∼25°C), and examples of living, brown-to-dark-green-colored, felted mats of photosynthetic cyanobacterium *Calothrix* spp. (**A**) Facies diagram of siliceous sinter hot-spring deposits with thin palisade lamination positioned on the distal apron (modified from Guido and Campbell, 2011). Inset below shows photomicrographs of palisade microtextures in stacked laminae comprising dense, vertically oriented filaments (dark) and primary porosity (white; some voids still empty while others filled with clear silica), from (left) Tahunaatara sinter (15 ka), Taupo Volcanic Zone (TVZ), New Zealand (*cf.* Campbell *et al.*, 2003), and (right) Healy's Bore 2 sinter apron at Tokaanu (see field photo in B), TVZ. (**B**) Typical field location of palisade fabric on an active siliceous hot spring sinter apron at Tokaanu, TVZ. Ct, *Calothrix* terracettes forming palisade fabrics (<40°C); gm, geothermal marsh reeds growing on apron margin at ambient temperatures; v, vent area sinter (intermittently >90°C). (**C**) View of active Fountain Paint Pots siliceous sinter apron, Yellowstone National Park, USA. ltCP&T, low-temperature (<40°C), brown-colored, felted to mamellated, photosynthetic cyanobacterial mats lining *Calothrix* pools and terraces in foreground; mtP, mid-temperature (∼45–55°C) pools with orange-to-green-colored, conical tufted mats of photosynthetic bacteria *Lyngbya* and/or *Oscillatoria* growing on pool floors in middle ground; mtDC, mid-temperature discharge channels with "bubble mats" of green and orange cyanobacteria lining channel bottom; htVG&PS, high-temperature vent geysers and proximal slope (>60°C) sinter deposits in the background, over which discharge channels flow. (**D**) Detail of *Calothrix*-lined pool and terrace rim, forming light brown–colored, mamellated, bushy encrustations constituting palisades sinter; oblique view; pencil for scale. (**E**) Further detail of *Calothrix* "puff balls" (light brown), actively accreting siliceous sinter (white), from location shown in (C, D); plan-view; coin (2 cm diameter) for scale. (Color graphics available at www.liebertonline.com/ast)

aprons, which archive shifting paleoenvironmental conditions in vent-to-distal apron gradients reflecting temperature (100°C to ambient), pH, and hydrodynamics (Fig. 1A; *e.g.*, Walter, 1976; Farmer and Des Marais, 1994; Cady and Farmer, 1996; Jones *et al.*, 1997a, 1997b, 1998; Lowe *et al.*, 2001; Guidry and Chafetz, 2002, 2003a, 2003b, 2003c; Lynne and Campbell, 2003; Handley and Campbell, 2011; Lynne, 2012). Siliceous sinters are utilized as analog representatives for ''extreme'' environmental conditions that may have prevailed on Earth and Mars billions of years ago, with hydrothermal systems having been implicated as possible crucibles for the origin and evolution of early life (*e.g.*, Bock and Goode, 1996; Stetter, 1996; Farmer and Des Marais, 1999; Farmer, 2000; Westall *et al.*, 2001, 2015; Konhauser *et al.*, 2003; Maliva *et al.*, 2005; Hofmann and Harris, 2008; Ruff *et al.*, 2011). Nonetheless, sinters undergo postdepositional mineralogical and physical changes, including diagenesis from opal-A to quartz (*e.g.*, Herdianita *et al.*, 2000a; Campbell *et al.*, 2001; Jones and Renaut, 2007; Lynne *et al.*, 2007), which may alter the preserved biosignals. Indeed, while some ancient sinter deposits retain many of their original macroscale and even microscale textural characteristics (*e.g.*, Trewin, 1993, 1996; Walter *et al.*, 1996; Guido *et al.*, 2010; García Massini *et al.*, 2012), secondary mineralization, late-stage cement infill, replacement, dissolution/reprecipitation, and acid-steam etching also result in patchy recrystallization or even destruction of original textures and biosignatures (*e.g.*, Campbell *et al.*, 2001; Jones *et al.*, 2001; Guidry and Chafetz, 2003a; Lynne and Campbell, 2003; Hinman and Walter, 2005; Campbell and Lynne, 2006; Campbell *et al.*, 2015). The factors controlling differential preservation in sinters are still uncertain, although early and rapid silicification is a key feature of biosignature preservation in both sinters and many fossiliferous Precambrian rocks (*e.g.*, Knoll, 1985; Trewin, 1996; Maliva *et al.*, 2005; Campbell *et al.*, 2015; Westall *et al.*, 2015).

One of the most voluminous hot-spring facies in the geological record is the low-temperature (<40°C), so-called palisade fabric affiliated with distal apron-slope settings in sinters and travertines. In present-day siliceous hot springs, this facies is found in low terracettes (<10 cm water depth,
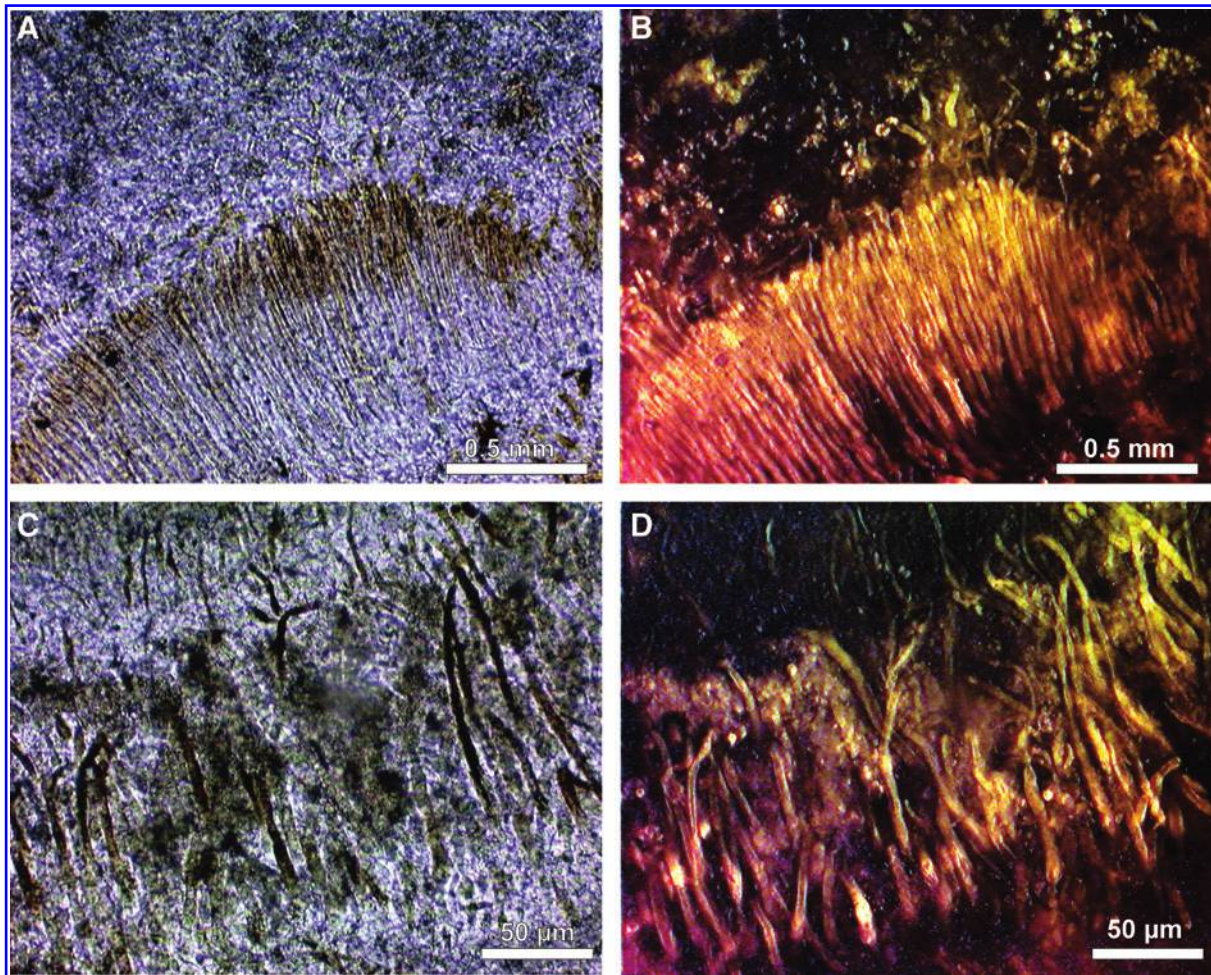

FIG. 2. Petrographic thin section photomicrographs of modern palisade fabric within sinter sampled at site M1 from Golden Fleece Terrace, Orakei Korako, TVZ (see Fig. 6A, 6C–6F). Laminae of vertically oriented, silica-encrusted, cyanobacterial sheaths forming a palisade sinter microfabric. Microbial horizons alternate with laminae of dark, porous, fenestral sinter. **(A)** Plane-polarized light. **(B)** Fluorescent light. **(C–D)** Detail of unstained petrographic thin section of modern sinter showing entwined, silica-encrusted, vertically oriented cyanobacterial sheaths in a palisade microfabric. (C) Plane-polarized light. (D) Fluorescent light. (Color graphics available at www.liebertonline.com/ast)
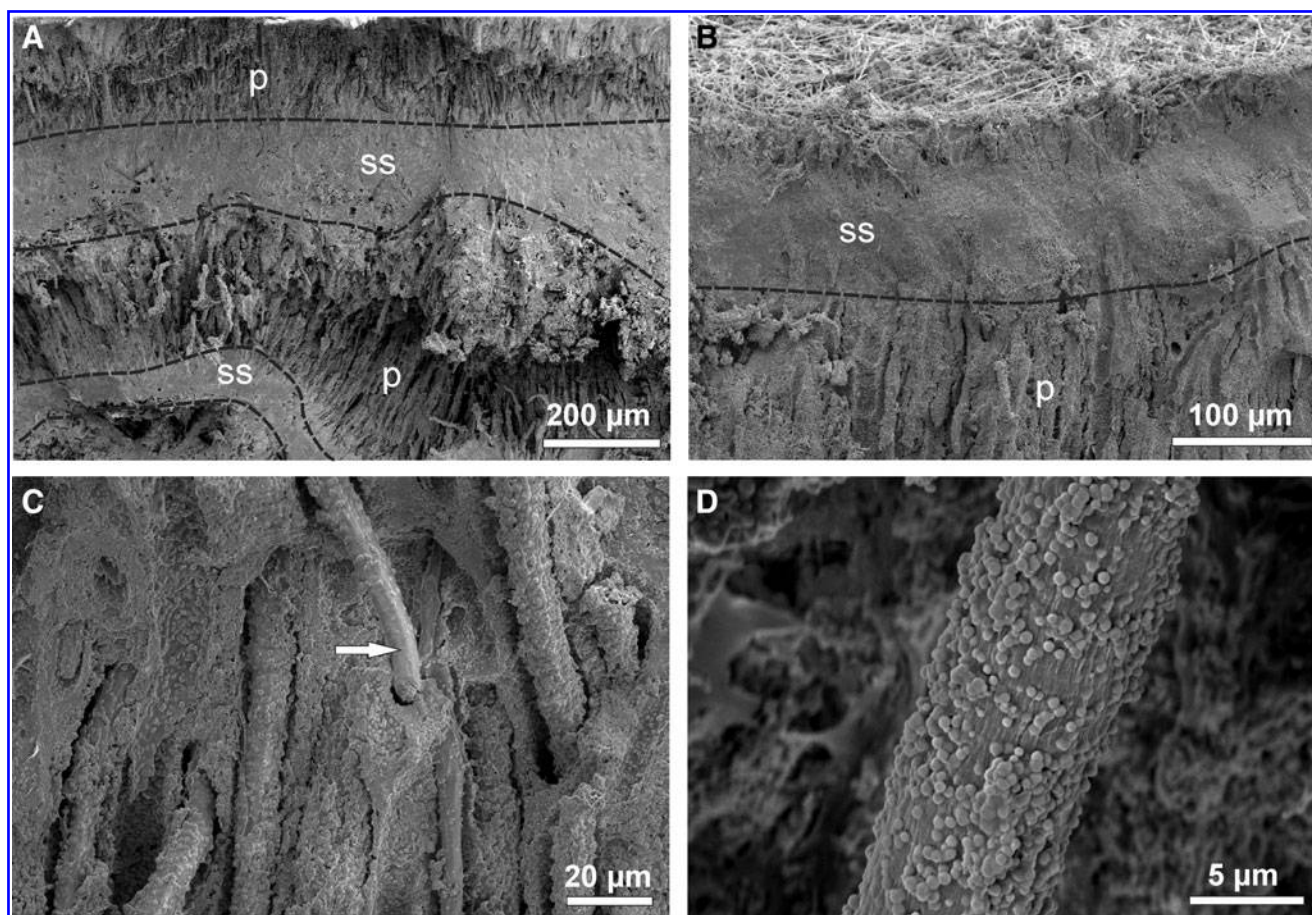
FIG. 3. Scanning electron microscope images of palisade fabric within modern sinter from Orakei Korako; sample M1. (**A**) Alternating horizons of smooth silica (ss) and densely packed, vertically oriented, cyanobacterial sheaths (p) that form the palisade sinter microfabric. (**B**) Uppermost horizon of filamentous fabric (p), $\sim 100\,\mu$m below the sinter surface, immediately underneath a smooth silica (ss) horizon. (**C**) Palisade microfabric shows silica-encrusted, subvertically oriented cyanobacterial sheaths. Arrow indicates filament sheath not coated with opal-A spheres. (**D**) Individual cyanobacterial sheath partially encrusted with $0.5\,\mu$m diameter opal-A silica spheres.

e.g., Fig. 1A, 1B) and larger terrace pools (up to ~ 0.5 m water depth, *e.g.*, Fig. 1C, 1D) that are dominated by brown-to-dark-green-colored, coarsely filamentous *Calothrix* spp., which are photosynthetic cyanobacteria of the Rivulariaceae family. The *Calothrix* genus represents a collection of phylogenetically diverse cyanobacterial species (Sihvonen *et al.*, 2007) that are capable of specialized cell differentiation, leading to heterocystous nitrogen fixation (*e.g.*, Stewart, 1962; Jones, 1992). *Calothrix* spp. are characterized by trichomes (up to $\sim 20\,\mu$m diameter) with tapered tips, which are encapsulated in sheaths ~ 10–$30\,\mu$m in diameter, ~ 1–4 mm long, with wall thicknesses of ~ 1–$8\,\mu$m (Watanabe and Kurogi, 1975). These filaments develop into closely packed, vertically oriented, micropillar structures (*e.g.*, Figs. 2–4; Cassie, 1989; Cady and Farmer, 1996; Lynne and Campbell, 2003). Palisade sinter fabrics from thermal springs typically comprise alternating laminae (1–5 mm thick) of filament-rich and solid silica horizons (*e.g.*, Fig. 3; Campbell *et al.*, 2001). The stacking of silicified, filamentous palisade horizons collectively constitutes stromatolitic buildups on distal sinter-apron terrace(tte)s (Fig. 1A, 1B). Upper surfaces of well-developed, felted mats of *Calothrix* display mamellated to shrubby morphologies in association with relatively calm,

subaqueous, thermal pool settings (Fig. 1C–1E). Palisade fabrics affiliated with microbial activity also have been recognized in other settings, such as tidal flat-associated carbonate sequences (*e.g.*, Eriksson and Truswell, 1974).

Weed (1889) was the first to recognize palisade textures in modern hot-spring environments at Yellowstone National Park (USA), which he described as ''fibrous'' layers of silica-encrusted ''algous vegetation.'' In Devonian sinters from the Drummond Basin, Australia, Walter *et al.* (1996, 1998) reported tubular microfossils with diameters of 5–$8\,\mu$m and 10–$12\,\mu$m, akin to thermal spring filament diameters characteristic of modern New Zealand examples. Palisade fabric in fossil hot-spring deposits also has been identified in the Devonian Windyfield chert, Scotland (Fayers and Trewin, 2003), Jurassic sinter in Patagonia (Guido and Campbell, 2009, 2011, 2014), and Quaternary sinters in the Taupo Volcanic Zone (New Zealand) at Umukuri (Campbell *et al.*, 2001), Tahunaatara (Campbell *et al.*, 2003), Mangatete (Drake *et al.*, 2014), Te Kopia (Lynne and Campbell, 2003), and Orakei Korako (Lynne and Campbell, 2003, 2004).

This study documents the character and preservation potential of the palisade facies throughout the mineralogical
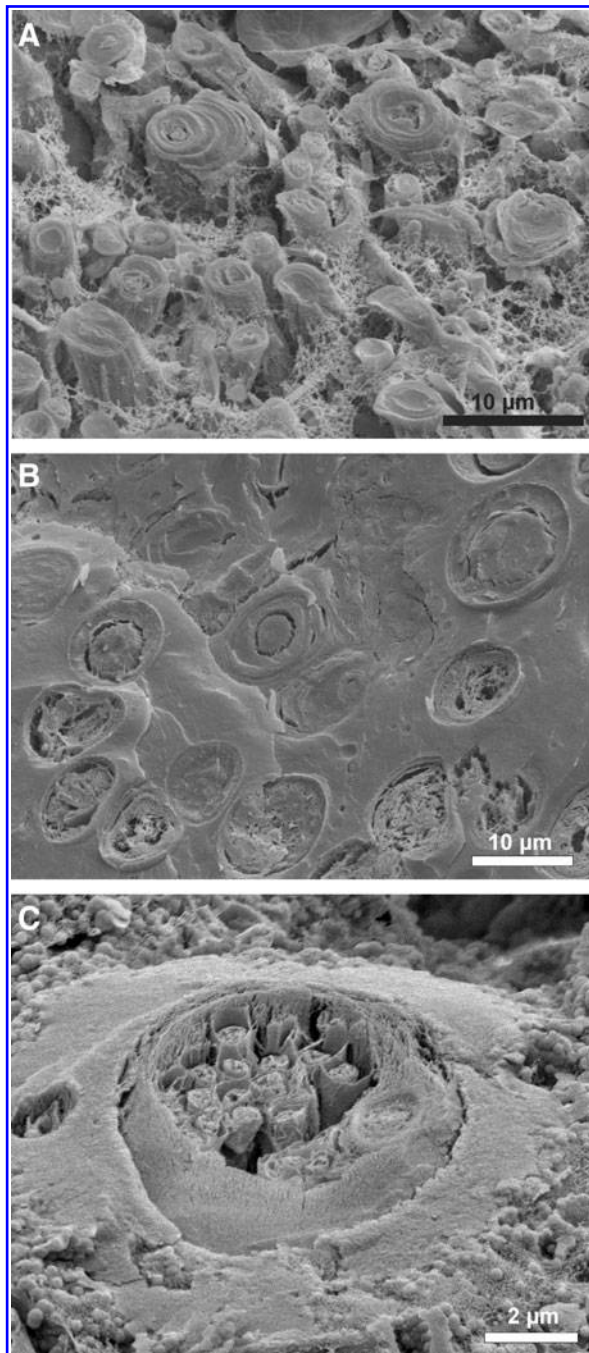
FIG. 4. Cryo–scanning electron microscope images showing characteristic morphology of modern microbial mat from a low-temperature thermal spring environment at Orakei Korako. (**A–B**) Cross-sectional view of closely packed, vertically oriented filaments, in viable (living) palisade mat from Orakei Korako. Exopolymeric substance (EPS) secreted by the microbes fills in pore space around filaments, producing a networklike (A) (desiccated; Handley *et al.*, 2008) or smooth (B) texture. (**C**) Increased magnification of coarse palisade filament with opal-A spheres beginning to silicify around the outer sheath surface.

maturation sequence in sinters, from living *Calothrix* with nascent encrustations of opaline silica in modern hot springs, to microfossils entombed in Late Jurassic (~150 Ma), low-temperature, quartzose sinter. Rock and biological samples from the palisade facies were analyzed by thin-section petrography, scanning electron microscopy (SEM, cryo-SEM), X-ray powder diffraction (XRPD), laser Raman spectrometry, molecular techniques, and lipid biomarker extraction. Collectively, they record snapshots of sinter maturation and allow for a systematic tracking of changes in biosignatures with diagenesis over geologically significant time intervals.

2. Field Settings

Palisade textures and microbiology were examined in detail from sinter collected on the actively accreting Golden Fleece and Rainbow terraces, Orakei Korako, Taupo Volcanic Zone (TVZ), New Zealand, and for comparison, from a small, low-temperature, spring-discharge channel at Kuirau Park, Rotorua, TVZ (Figs. 5 and 6; Jordan, 2007). Some of these modern, brown to dark green mats (29–39°C) were analyzed for their molecular and/or lipid biomarker signatures (Figs. 6–8). In addition, four TVZ Holocene (fossil) sinter deposits and one Jurassic, palisade-bearing sinter sample (~150 Ma) from the Deseado Massif, Argentine Patagonia, were evaluated in this study. Sample locations and descriptions of TVZ samples are listed in Tables 1 and 2, and the geological context and texture of the Jurassic sinter sample from Patagonia is illustrated in Fig. 9.

The Orakei Korako geothermal field is situated 37 km southwest of Rotorua and 25 km north of Taupo (Fig. 5A). Hochstetter (1864) was the first to describe the geothermal activity, with updates provided by Lloyd (1972) and Hamlin (1999). Surficial thermal activity (~1.8 km^2) constitutes hot springs, geysers, mud pools, fumaroles, and extensive active and inactive siliceous sinter terraces, with most thermal features occurring along about 1 km of the eastern shoreline of Lake Ohakuri (Waikato River), in and adjacent to the main tourist area at Orakei Korako (Lloyd, 1972; Simmons and Browne, 1991; Hamlin, 1999). In 1961, the Waikato River was dammed 9 km downstream of Orakei Korako for hydroelectric power development, raising the water level by 18 m and flooding approximately 70% of the active thermal features beneath the surface of Lake Ohakuri (Lloyd, 1972). The local geology was documented in detail by Lloyd (1972), Steiner (1977), and Bignall (1991, 1994). The stratigraphy consists of a sequence of flat-lying felsic ignimbrites, air fall tuffs, and reworked equivalents (Simmons and Browne, 1991). The first detailed study of sinter textures at Orakei Korako was by Renaut *et al.* (1996), who described siliceous oncoids indicative of wetting and drying periods on the fault-bound apron terraces. Lynne and Campbell (2003) documented diagenetic transformations from opal-A to quartz within low-temperature microbial textures from several TVZ fields including Orakei Korako. Morphological and mineralogical transitions from opal-A to opal-CT in low-temperature siliceous sinters at Orakei Korako and Te Kopia were reported by Lynne and Campbell (2004). In addition to the actively forming sinter at Orakei Korako, fossil sinter sheets and terraces (456–6276 years BP, unpublished ^{14}C dates) are extensive at both Orakei Korako and Umukuri 1 km to the southwest (Fig. 5), with most old sinter terraces at Orakei Korako found at higher elevations (up to about 10 m) than the presently forming sinters. At the southernmost mapped extent of the greater Orakei Korako area, Sinter Island (456 years BP; Campbell and Lynne, 2006) is situated within Lake Ohakuri, approximately 40 m
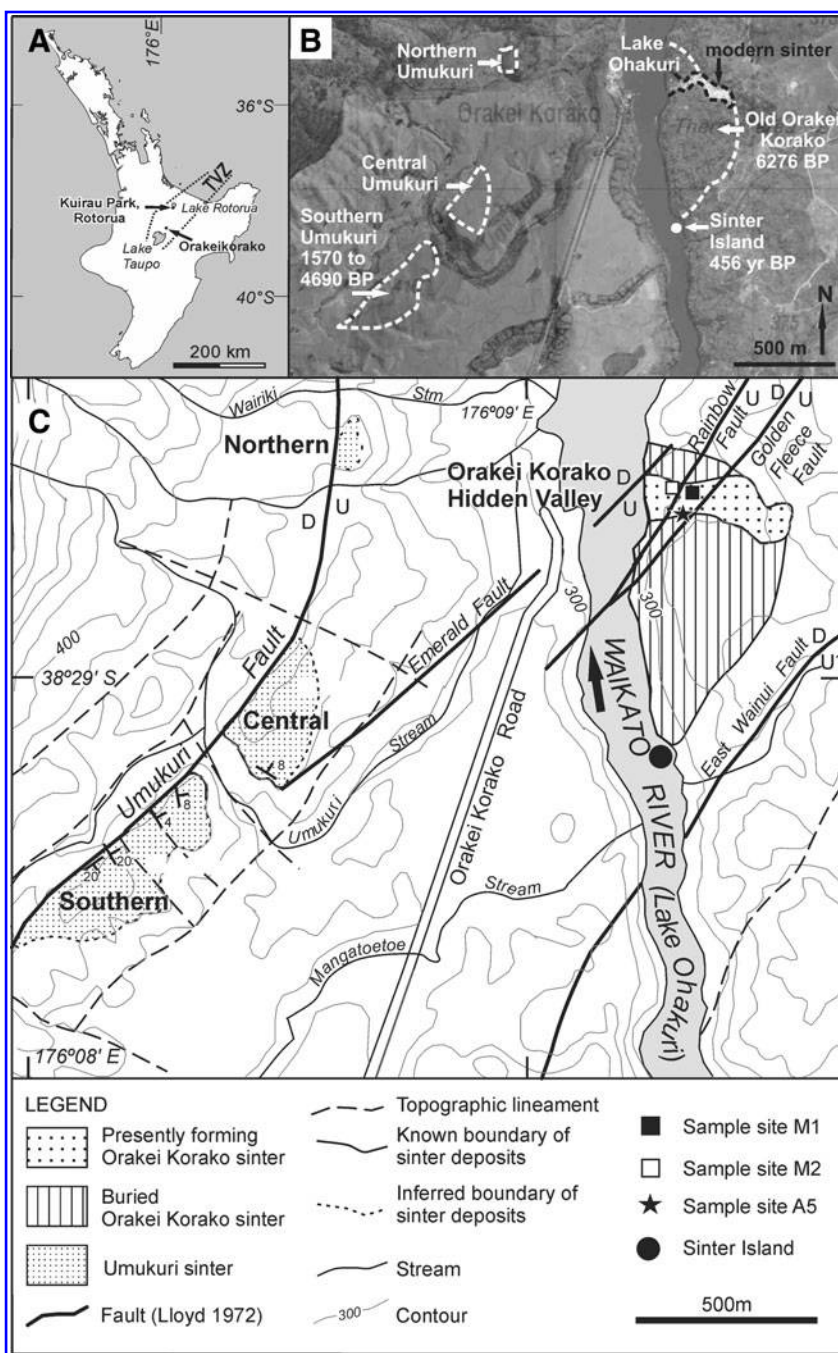
FIG. 5. Location map of Orakei Korako geothermal area and fossil Umukuri sinter. (**A**) Position of Orakei Korako within the TVZ, North Island, New Zealand. (**B**) Sketch map overlain on Google Earth image indicating location of sample sites at Orakei Korako. (**C**) Sinter distribution map showing location of sinter at Orakei Korako and Umukuri with respect to Lake Ohakuri (Waikato River) and local faults.

from its eastern bank and ∼700 m south of the main tourist area (Fig. 5B, 5C). The bush-clad, triangular island (7 × 10 m in areal extent) comprises relatively flat-bedded sinter (3–3.5 m thick), with a few domal stromatolites exposed on its western margin and vent geyserite on its eastern side.

Thermal activity at Orakei Korako is fault-controlled (Lloyd, 1972; Bignall, 1991; Simmons and Browne, 1991). Northeast splays of a major, normal, eastern boundary fault of the TVZ, the Paeroa Fault, dissect Orakei Korako with downward displacement of several meters to the west (Fig. 5C; Simmons and Browne, 1991). Prior to the 186 AD Taupo super volcano eruption, seismic movement along the Paeroa Fault zone caused spring discharge from the East

Wainui Fault to cease, with new springs subsequently developing along traces of the Emerald, Rainbow, and Golden Fleece faults (Simmons and Browne, 1991). Today, the fault scarps are draped with siliceous sinter and form a series of stepped terraces. The main upflow is located to the north, with a southerly outflow toward Lake Ohakuri (Sheppard and Lyon, 1984).

The Umukuri sinter (∼0.8 km² areal extent, 12 m maximum thickness; Campbell et al., 2001) comprises several outcrops representing mid- to low-temperature aprons that occur discontinuously for 1.6 km along the upthrown eastern scarp of the Umukuri Fault, 1 km to the southwest of Orakei Korako (Fig. 5C). Based on field relationships, including
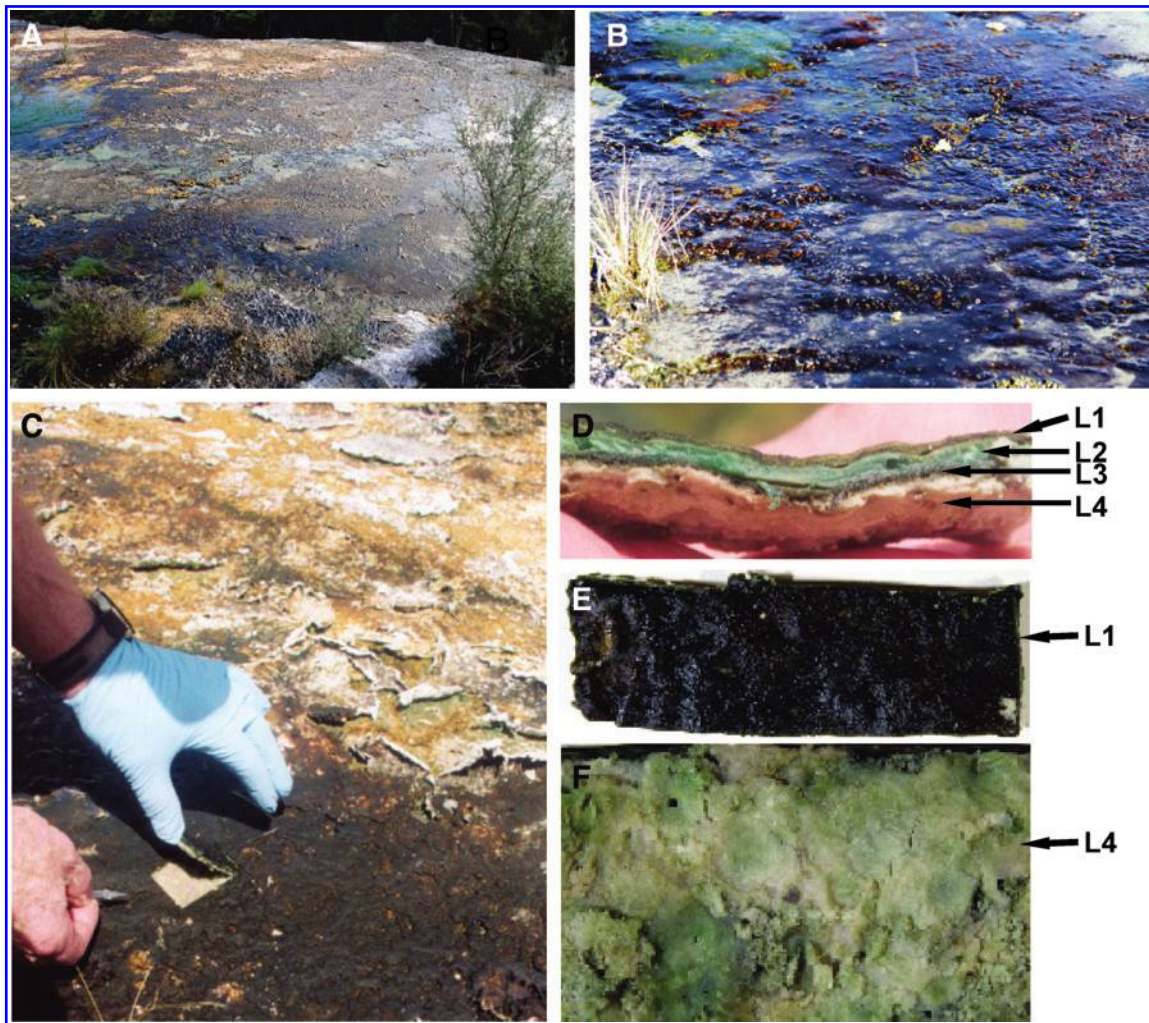
FIG. 6. Sampling fresh palisade samples at Orakei Korako. (**A**) Location of sample site M1 on Golden Fleece Terrace. (**B**) Location of sample site M2 on Rainbow Terrace. (**C**) Cutting out a section of fresh, dark green, low-temperature, palisade mat on Golden Fleece Terrace at M1. (**D**) Cross-sectional view of fresh palisade mat and underlying sinter horizons L1–L4 at site M1. (**E**) Uppermost surface (L1) of fresh palisade mat at M1. (**F**) Sinter horizon (L4) immediately underneath the living dark-green-to-brown-colored palisade mat sampled at M1. (Color graphics available at www.liebertonline.com/ast)

paleo-ripple directions on sinter surfaces, Lloyd (1972) hypothesized that the Umukuri sinter represents an older manifestation of surface hot-spring discharge in the Orakei Korako geothermal field, with geothermal activity migrating eastward over time. While he reported that active hot

FIG. 7. Relative proportions of bacterial OTUs in modern microbial mat samples. Minor OTUs are combined into the category ''Other.'' (Color graphics available at www .liebertonline.com/ast)

springs were present in 1961 at southern and northern Umukuri, with mud pools and active steam vents found to the north, there is no such activity evident in the Umukuri area today. Umukuri fossil sinter outcrops range in age between 1570 and 4690 yrs BP (unpublished ^{14}C data) and therefore are much younger than earlier reported age estimates based on stratigraphy (Campbell *et al.*, 2001; Lynne and Campbell, 2003).
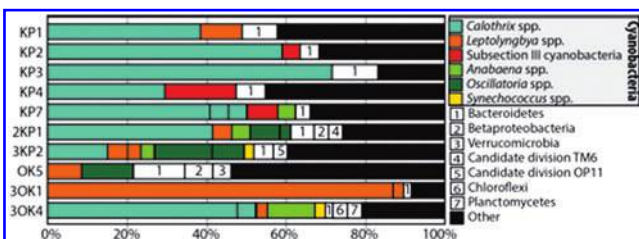
In Argentine Patagonia, the Claudia hot spring area is one of 23 fossil geothermal localities discovered in the Jurassic volcanic-hydrothermal Deseado Massif province (Fig. 9A; Guido and Campbell, 2011). In the Middle-Late Jurassic ($\sim$178–151 Ma; Pankhurst *et al.*, 2000), the Deseado Massif area was affected by mostly rhyolitic and andesitic volcanism, owing to crustal thinning in a diffuse extensional back arc setting affiliated with the breakup of Gondwana and opening of the South Atlantic Ocean (Riley *et al.*, 2001; Richardson and Underhill, 2002). Widespread hydrothermal activity was associated with the late volcanic phase in the Late Jurassic, which produced metalliferous epithermal

FIG. 8. Biomarker abundances within profiles of the mat sample shown in Fig. 6D. (**A**) Vertical distribution of cyanobacterial lipids through the microbial mat (L1–L3) and the newly formed sinter beneath (L4). Alkenes are denoted by the total number of carbon atoms, and the number of double bonds is indicated by the number that follows the colon. (**B**) Vertical distribution of *Chloroflexus* lipids through the microbial mat (L1–L3) and the newly formed sinter beneath (L4). (Color graphics available at www.liebertonline.com/ast)
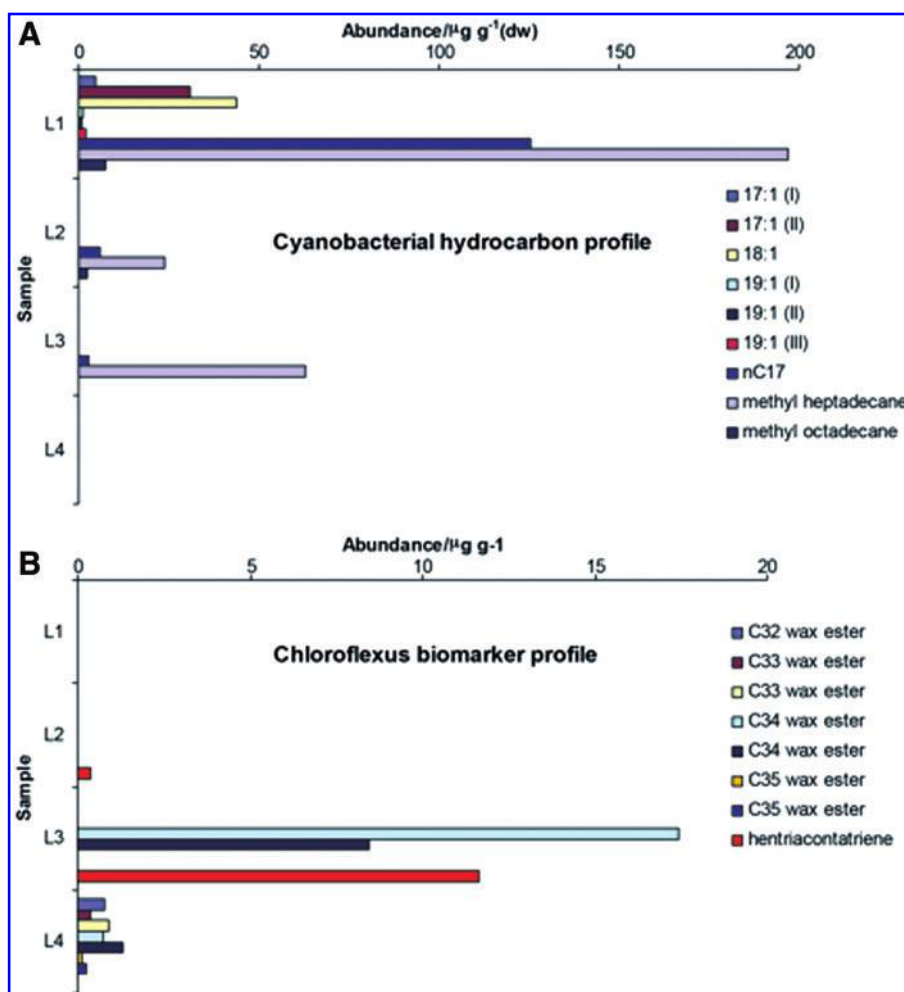
deposits (mainly Ag, Au), extensive silicification, and manifestation of geothermal features at the surface (Schalamuk *et al.*, 1997; Guido and Campbell, 2011).

The Late Jurassic Claudia geothermal field is geographically and geologically linked to the Cerro Vanguardia mine

TABLE 1. SAMPLES COLLECTED FROM KUIRAU PARK AND ORAKEI KORAKO FOR MICROBIOLOGICAL ANALYSES

Sample	Date collected	Location	Texture	Temp °C	pH
KP1	2-Sept-03	Kuirau Park	FM	37	9
KP2		Kuirau Park	FM	37	9
KP3		Kuirau Park	FM	37	9
KP4		Kuirau Park	FM	37	9
KP7		Kuirau Park	FM	39	9
2KP1	22-Jan-06	Kuirau Park	FM	30	9
3KP2		Kuirau Park	CT	38	9
OK5		Orakei Korako	FM*	29	7
3OK1	29-Mar-06	Orakei Korako	MM	38	9
3OK4		Orakei Korako	FM	36	9

KP, Kuirau Park; OK, Orakei Korako; CT, conical tufts; FM, felt mat; MM, mucilaginous mat.

*Medium brown felt mat within a few centimeters of a higher-temperature white mat.

(total resource of ∼7.8 million ounces Au equivalent) via proximity, similar veins, and structural linkages, making it an especially relevant prospect for the region (Fig. 9B; Guido and Campbell, 2014). Claudia is one of the largest (40 km²) and most paleoenvironmentally varied hot-spring deposits in the Deseado Massif, containing fluvially reworked, inferred hydrothermal silica gels, extensive apron terraces, and a clustering of high-temperature subaerial vent mounds. There are two diagnostic outcrops: La Calandria Sur and Loma Alta (Fig. 9B). La Calandria Sur is mainly characterized by sinter and travertine occurring in the same stratigraphic sequence, along with well-preserved, structurally controlled geyserite outcrops (Guido and Campbell, 2014; Campbell *et al.*, 2015). Loma Alta constitutes only low outcrops and *in situ* blocks of sinter, but with extraordinary preservation of the textures, possibly because of early diagenesis. Diagnostic fabrics of the Loma Alta sinter include hydrothermal breccias (inferred to indicate proximity to vent conduits), geyserite, wavy laminated, bubble mat, and palisade fabrics, allowing definition of a proximal to low-temperature gradient sinter facies association for the area. The site was used in this study as an example of Jurassic palisade texture, with sample C105 comprising a laminated sinter with several patches of extraordinary preservation of microbial fabric (Fig. 9C–9E).

TABLE 2. X-RAY POWDER DIFFRACTION (XRPD) RESULTS OF ROCK SAMPLES CONTAINING PALISADE FABRIC

Location	Sample number	FWHM (°2θ)	FWHM (Å)	MI (c/s)	Apex (°2θ)	Silica phase
Modern OK	M2 (sinter under mat)	8.05	1.39	80	22.2	Opal-A
Modern OK	M1 (layer 4)	7.5	1.29	81	22.3	Opal-A
Old OK	A1701porous	7.0	1.25	84	22.4	Opal-A
Old OK	A1701aporous	6.75	1.17	85	22.2	Opal-A
Old OK	A1702white	7.55	1.32	87	22.35	Opal-A
Old OK	A1701porous r2	7.0	1.25	84	22.4	Opal-A
Old OK	A1801porous	7.0	1.25	81	22.1	Opal-A
Old OK	A1802white	6.75	1.20	83	22.1	Opal-A
Old OK	A1803grey	7.2	1.30	80	22.35	Opal-A
Old OK	A2whitevit	7.55	1.33	84	22.2	Opal-A
Old OK	A12infill	7.1	1.27	76	22.2	Opal-A
Old OK	A2pal	7.4	1.30	83	22.2	Opal-A
Old OK	A12porous	7.4	1.30	74	22.2	Opal-A
Old OK	A13porous	7.5	1.31	82	22.15	Opal-A
Old OK	A13infill	7.7	1.37	79	22.2	Opal-A
SI	A2003	6.55	1.20	98	21.55	Opal-A
SI	A21	6.4	1.14	88	22.0	Opal-A
SI	A2001	5.35	0.96	103	21.5	Opal-A/CT
SI	A4brown	2.0	0.41	190	21.6	Opal-CT
Old OK	A502	0.80	0.15	465	21.75	Opal-CT
Old OK	A503	0.75	0.14	510	21.65	Opal-CT+m
Old OK	A503repeat	0.8	0.16	498	21.6	Opal-CT
SI	A22brown	2.5	0.47	144	21.9	Opal-CT
SI	A4white	1.5	0.28	239	21.75	Opal-CT
SI	A22white	0.7	0.12	270	21.7	Opal-C+q+m
SI	A22pink	1.5	0.29	268	21.7	Opal-C+q
SI	A24brown	0.8	0.15	250	21.75	Opal-C+q
Umukuri	A1601	0.65	0.12	470	21.8	Opal-C+q+m
Umukuri	A1602	0.60	0.11	620	21.75	Opal-C+q
Umukuri	A1603	0.65	0.12	410	21.8	Opal-C+q
Umukuri	A701	0.6	0.11	540	21.8	Opal-C+q
Umukuri	A702	0.6	0.11	595	21.8	Opal-C+q
Umukuri	A703	0.5	0.09	690	21.9	Opal-C+q
Umukuri	A901grey	0.75	0.14	470	21.75	Opal-C+q+m
Umukuri	A902porous	0.6	0.11	551	21.75	Opal-C+q
Umukuri	A903white	0.8	0.15	445	21.9	Opal-C+q
Umukuri	A1001	0.6	0.11	609	21.8	Opal-C+q+m
Umukuri	A1002porous	0.7	0.13	555	21.75	Opal-C+q
Umukuri	A1003old detector	0.65	0.12	534	22.0	Opal-C+q
Umukuri	A1003 rep	0.55	0.10	596	21.75	Opal-C+q
Umukuri	A1003r3	0.55	0.10	585	21.75	Opal-C+q
Umukuri	A1003newdetector	0.50	0.11	550	21.75	Opal-C+q
Umukuri	A1003r4	0.55	0.10	565	21.75	Opal-C+q
Umukuri	A1003r5	0.6	0.11	580	21.75	Opal-C+q
Umukuri	A11	0.7	0.13	488	21.9	Opal-C+q+m
Umukuri	A1	0.85	0.13	21.75	200	Opal-C+q
Umukuri	A1401translucent	0.25	0.05	440	20.9	Quartz
Umukuri	A1402white	0.25	0.05	500	20.9	Quartz+m
Umukuri	A1402white	0.2	0.04	500	20.9	Quartz

OK, Orakei Korako; SI, Sinter Island; m, moganite; q, quartz.

3. Methods

3.1. Overview

Brown to dark green felted mats of presumed *Calothrix* affinity were sampled on active, distal sinter apron terraces for molecular, lipid biomarker, and SEM study in order to characterize living mat features—the biological baseline upon which silica templates and all subsequent modification takes place. The mineralogical-morphological changes ac-companying silica diagenesis in the transition from opal-A to quartz were analyzed on TVZ sinter samples using XRPD, SEM, and standard thin section microscopy. Jurassic samples were studied by optical microscopy and laser micro-Raman spectrometry to confirm the occurrence of carbon in palisade textures embedded in quartz. This multi-technique approach enabled mineralogical, textural, and biological signatures to be traced through the silica phase maturation sequence into the geological record.
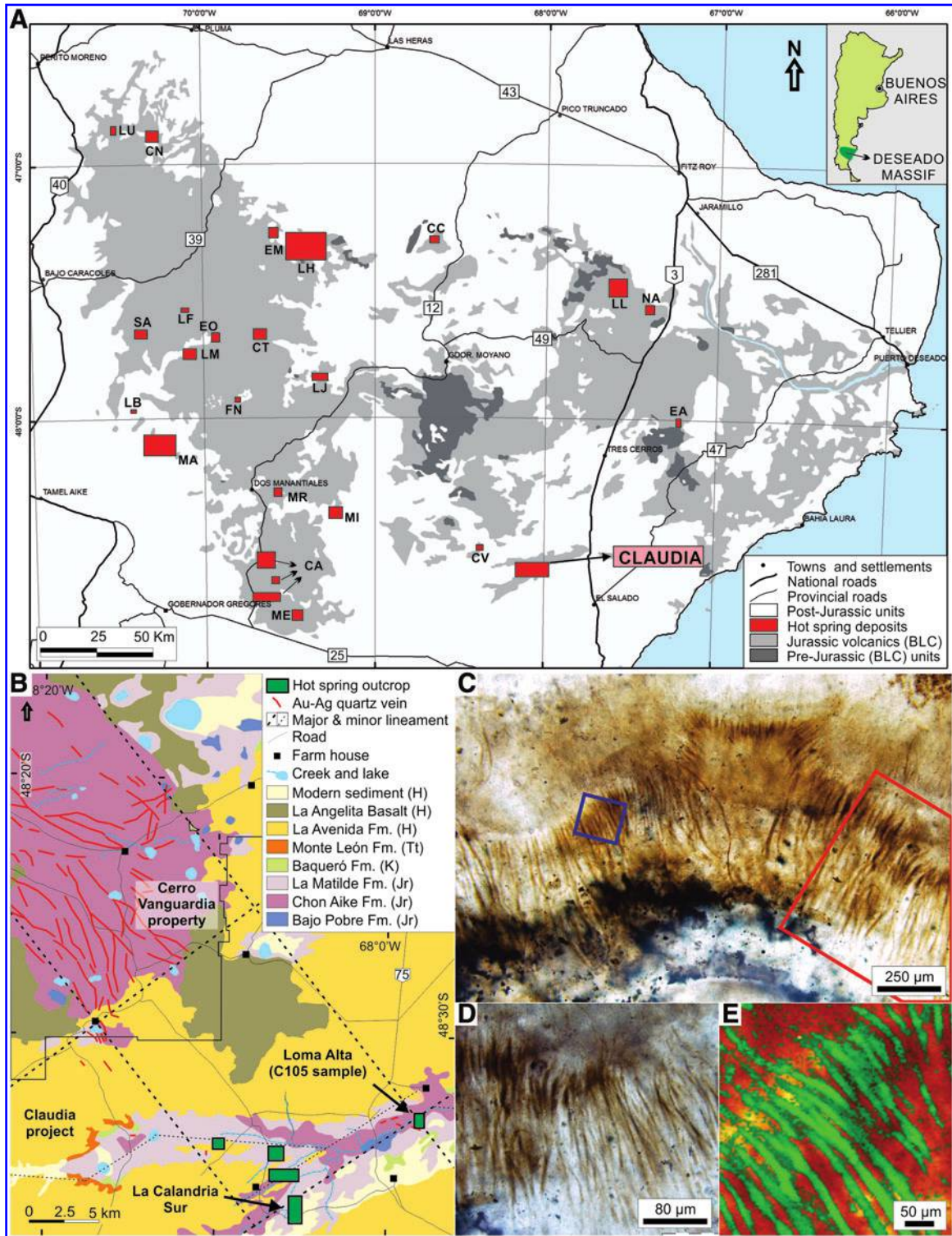
FIG. 9. Locality and geological map of the Late Jurassic (∼150 Ma) Claudia sinter and sample (C105) of fossil palisade fabric. (**A**) Hot-spring deposits (red boxes) in the Deseado Massif volcanic province, with the Claudia paleo-geothermal system shown in the southeastern portion of the massif. Double-letter labels refer to name abbreviations of the other 22 known systems (listed in Guido and Campbell, 2014; regional Deseado Massif context is described in Guido and Campbell, 2011). Volcanic units of the Bahía Laura Complex (BLC), associated with breakup of Gondwana and opening of the South Atlantic Ocean, are shown in gray shading. (**B**) Local geological context of Claudia hot-spring outcrops (green boxes), and locations of Cerro Vanguardia and Claudia epithermal veins, and the site where studied sample C105 was collected. (**C**) Densely packed subvertical to vertical tubular microfossils (reddish brown in color) in a filamentous horizon (up to 0.5 mm thick) with generally excellent preservation quality. Red box indicates location of photomicrograph in (D), and blue box shows location of Raman map in (E). (**D**) Detail of fossil palisade mat horizon [shown in (C), red box]. (**E**) Laser micro-Raman image of filamentous palisade fabric [shown in (C), blue box]: green = carbon; yellow/orange = quartz. (Color graphics available at www.liebertonline.com/ast)

3.2. Molecular analyses

3.2.1. Collection of modern mat samples for molecular analysis. A total of 10 representative samples (Table 1) were collected from zones of dark brown microbial mat growing in shallow geothermal vent outflow fluids at Kuirau Park (~18 m long triple vent outflow channel at central eastern edge of the park) and at Emerald Terrace (Orakei Korako). Both sites are silica-depositing, near-neutral alkali-chloride systems within the TVZ. Samples were collected from mats submerged in fluids with sterile tweezers, stored in sterile 15 mL polypropylene tubes, and transported on ice before storage at −20°C. Water temperature was measured with a ST80 XB ProPlusTM noncontact infrared temperature measurement gun with laser targeting sighting (Raytek, CA, USA). Fluid pH was measured to within 0.5 pH units using Panpeha Plus strips with a pH range of 0–14 (Schleicher & Schuell MicroScience GmbH, Germany). Samples KP1–KP4 were replicate samples collected from the same region of a brown microbial mat, while KP7 was collected from a region ~2 m up-gradient.

3.2.2. DNA extraction. Total genomic DNA was extracted in the School of Biological Sciences, University of Auckland (UOA) with a direct lysis bead beater method modified from Miller *et al.* (1999). Approximately 500 mg of sample was combined with 270 μL of sodium phosphate buffer and 30 μL of Lysozyme (10 mg/mL), and homogenized by vigorous vortexing and pipetting. After incubation at 37°C for 1 h, 300 μL of SDS lysis buffer was added. Contents were transferred to a 2 mL polypropylene bead beater vial containing 0.5 g each of 0.1 and 2.5 mm zirconia/silica beads (bioSpec Products, Inc.). To this, 300 μL of chloroform-isoamyl alcohol (24:1) was added, and vials were shaken in a FastPrep FP120 (Savant) machine at 4.0 m/s for 40 s. Beating was repeated after 1 min of cooling. Cell debris were pelleted, and the supernatant was combined with ammonium acetate (final concentration 2.5 *M*). The solution was mixed gently and then centrifuged for 5 min. The resulting clear supernatant was combined with 0.54 volumes of isopropanol and incubated at room temperature for 15 min. DNA was pelleted and washed with 1 mL of 70% ethanol, and then suspended in 50 μL of dH$_2$O. DNA was quantified with a NanoDrop ND-100 UV-vis spectrophotometer and stored at 4°C.

3.2.3. PCR amplification of bacterial 16S rRNA genes. Universal bacterial primers PB36 and PB38 (Saul *et al.*, 2005) were used to amplify bacterial 16S rRNA genes from positions 8 to 1509. PCR reactions were performed in 50 μL volumes containing 1×PCR buffer (20 m*M* Tris-HCl, pH 8.4, 50 m*M* KCl), 2 m*M* MgCl$_2$, 100 μM dNTPs, 0.2 μM each of PB38 and PB38, 1.0 U PlatinumTaq (Invitrogen), and 2 μL of DNA template of a concentration between 1 and 10 ng/μL. PCR cycling conditions were 94°C for 3 min, 25 cycles of 94°C for 45 s, 55°C for 45 s, and 72°C for 90 s. PCR reactions were carried out in an Eppendorf Mastercycler Gradient PCR machine or a Biometra Thermocycler using default ramping parameters. PCR products were analyzed by electrophoresis on 1% (w/v), 0.5×TBE agarose gels, run at 120 V for 15–20 min.

3.2.4. Clone library construction. Prior to cloning, PCR products were purified using the Roche High Pure PCR Product Purification kit following the manufacturer's instructions, and quantified by NanoDrop. Ligations were performed in reaction volumes of 10 μL with the pGEM-T Easy vector system 1 (Promega) according to the manufacturer's instructions. Insert-to-vector ratios of 3:1 were used, and ligations were incubated overnight at 4°C. Transformations were performed using Library Efficiency DH5α competent cells (Invitrogen) in 15 mL falcon tubes. Cells were thawed on ice and 5 μL of ligation mix added to 50 μL of cells, which were then incubated on ice for 25 min. The cells were heat shocked at 42°C for 50 s and then placed on ice for 2 min. Following this, 900 μL of room-temperature L-broth was added and the samples incubated on a roller at 37°C for 1 h. The transformation mix was then plated, in 300 μL aliquots, onto 15 cm L-agar plates containing ampicillin (125 μg/mL), IPTG (23 μg/mL), and X-Gal (33 μg/mL). Plates were incubated overnight (16–20 h) at 37°C.

White colonies were randomly picked into 96-well microtiter plates containing 150 μL of L-broth and ampicillin (125 μg/mL) and incubated overnight (16–20 h) at 37°C. Each library consisted of 96 clones. After incubation, 5 μL of each culture was transferred onto Whatman Clonesaver Cards and air-dried for 1 h. PCR using vector-specific primers was used to recover inserts from crude cell lysates. Lysates were prepared from overnight cultures by adding 50 μL of culture to 100 μL of dH$_2$O, incubating at 94°C for 30 min, and snap chilling on ice to lyse cells. PCR reactions were performed in 20 μL volumes containing 1×PCR buffer (as described above), 2.0 m*M* MgCl$_2$, 100 μM dNTPs, 0.2 μM each of pGEM-F (GGC GGT CGC GGG AAT TCG ATT) and pGEM-R (GCC GCG AAT TCA CTA GTG ATT), 0.5 U of Recombinant *Taq* DNA Polymerase (Invitrogen), and 2 μL of cell lysate. Cycling conditions used were 94°C for 3 min then 25 cycles of 94°C for 45 s, 55°C for 45 s, and 72°C for 90 s.

3.2.5. Restriction fragment length polymorphism (RFLP) of clones. The restriction endonuclease *Hae*III (Invitrogen) was used to generate RFLP profiles of the inserts. Digestions were performed by adding 5 μL of enzyme mix containing 1×REact 2 buffer (50 m*M* Tris-HCl, pH 8.0, 10 m*M* MgCl$_2$, 50 m*M* NaCl) and 10 U of *Hae*III enzyme to 20 μL of PCR product. The reaction mix was incubated for 3–12 h at 37°C. Digestion products (5 μL from each) were mixed with loading buffer and resolved by polyacrylamide gel electrophoresis (PAGE) on 17.4×0.1×8.7 cm (48 wells) 6% nondenaturing gels. Gels were run at 120 V for 70 min, stained in ethidium bromide/TBE solution for 10 min, and viewed under UV light. Each unique fingerprint profile was defined as an operational taxonomic unit (OTU), and OTU frequencies were calculated for each library.

3.2.6. Sequencing and analysis. Inserts were recovered from the plasmids of representative clones by PCR and purified as described above. Purified PCR products were sequenced by Macrogen Inc. (Kumchun-ku, Seoul, South Korea) in both forward and reverse directions with pGEM-F and pGEM-R primers, using a 3730×1 DNA Analyzer (Applied Biosystems). Forward and reverse sequences were

aligned and edited with ABI Autoassembler 2.0 (Applied Biosystems) or Vector NTI Advance 9.0 software (Invitrogen Life Technologies, CA, USA) to obtain consensus sequences. Consensus sequences were compared with GenBank database sequences using BLASTN (Altschul *et al.*, 1990).

3.3. Lipid biomarker extraction and analysis

3.3.1. Samples and sectioning for biomarker analysis. Lipid analysis was performed at the Imperial College (London) on two modern felt-textured, dark green-brown temperate mat and sinter samples that were collected at Orakei Korako from Golden Fleece Terrace (M1, Fig. 6A, 6C–6F) and Rainbow Terrace (M2, Fig. 6B), and a relict palisade sinter from Golden Fleece Terrace (A5) (Fig. 5C). The modern sample from M1 was divided into four distinct layers for analysis. Layers L1–L3 constituted the microbial mat, where L1 was the uppermost layer, and L4 comprised the deepest layer of newly formed sinter (Fig. 6D). The ancient relict sinter (A5) was undivided.

3.3.2. Saponification. For saponification, C19 *n*-alkane (200 ng) in hexane was added as an internal standard to the acid and polar (phospholipid) fractions. An aliquot (50%) of each sample was saponified by using methanolic sodium hydroxide (1 mL, 0.5 *M*, 70°C, 1 h). Samples were extracted with hexane, and the extracts were combined and evaporated under nitrogen into a Pyrex culture tube. Samples were then methylated with BF3–methanol (70°C, 1 h), and the methyl esters were extracted with chloroform. Finally, samples were concentrated to dryness, redissolved in chloroform, and eluted through a sodium sulfate column by using DCM to remove water. It is generally assumed that hydrolysis of the polar fraction releases predominantly fatty acids present as phospholipids; however, this fraction is analytically defined, and it is possible that hydrolysable components other than phospholipids are present.

3.3.3. Gas chromatography (GC) and gas chromatography–mass spectrometry (GC-MS). Before analysis, all fractions were silylated with pyridine and BSTFA (25 mL pyridine and 25 mL BSTFA, 70°C, 1 h) to convert alcohols into trimethyl silyl derivatives. Samples were analyzed with a Carlo Erba Instruments HRGC 5300 Megaseries gas chromatograph equipped with a Chrompack CP SIL-5CB capillary column (50 m ×0.32 mm internal diameter; 0.12 mm film, dimethylpolysiloxane equivalent) and a flame ionization detector. Hydrogen, at a head pressure of 10 psi, was used as the carrier gas, and samples were injected at 70°C with a temperature program of 20°C/min to 130°C and 4°C/min to 300°C and held for 20 min. GC-MS was performed with a Thermo Finnigan Trace gas chromatograph interfaced to a Trace mass spectrometer. The gas chromatograph column and temperature program were the same as those for GC analysis, although He was used as the carrier gas. Acquisition of data started 5 min after sample injection by autosampler. Electron ionization (70 eV) was used, and full scan spectra were obtained by scanning the range *m/z* 50–800 at 1 scan/s.

3.4. Mineralogical analysis

3.4.1. X-ray powder diffraction (XRPD). Five silica phases from immature, noncrystalline opal-A and opal-A/

CT, to paracrystalline opal-CT and opal-C+quartz, to mature microcrystalline quartz are present in varying amounts in TVZ siliceous sinter deposits (Fig. 10). XRPD is the principal technique used to determine the silica phase present and to compare the degree of lattice order among samples. XRPD analysis of samples was undertaken in the School of Environment (UOA) with a Phillips diffraction goniometer fitted with a graphite monochromator, with acquisition controlled by Sietronics (1993) VisXRD software. XRPD operating conditions were 40 kV and 20 mA, using CuKα radiation ($\lambda\alpha1 = 1.54051$ Å). Dry, untreated samples were scanned at 0.6° 2θ/min, with a step size of 0.01°, from 10–40° 2θ. Interpretation of the XRPD traces followed the technique outlined by Herdianita *et al.* (2000b). The full width at half maximum (FWHM) of the distinctive ∼2.2° 2θ (∼4 Å) diffraction band is a measure of the degree of lattice ordering within each phase (Herdianita *et al.*, 2000b). Lattice ordering increases with maturation, from noncrystalline opal-A and opal-A/CT to paracrystalline opal-CT and opal-C, and eventually to microcrystalline quartz. FWHM values of ∼8.0° 2θ are characteristic of immature opal-A, whereas values of ∼0.2° 2θ are typical of microcrystalline quartz (*cf.* Lynne *et al.*, 2005). As a reference, prominent diffraction bands for opal-A are centered at ∼22.2° 2θ (∼4 Å) for opal-A/CT, at 21.75° 2θ (4.09 Å) for opal-CT and opal-C, and at 20.85° 2θ (4.257 Å) for quartz (Jones and Segnit, 1971; Flörke *et al.*, 1991; Graetsch, 1994; Smith, 1998; Lynne and Campbell, 2003, 2004; Lynne *et al.*, 2005, 2007).

Forty-seven horizons within 19 samples were analyzed by XRPD for this study (Table 2). Bulk rock analyses and individual horizons within samples bearing varied textures also were extracted and analyzed. Six repeat runs of freshly sampled opal-C+quartz sinter were made to assess precision. All six runs produced FWHM values of $0.57 \pm 0.08°$ 2θ (0.11 ± 0.01 Å). The mean maximum intensity was 586 c/s, and the mean apex position was 21.75° 2θ. Accompanying the changing XRPD traces for various silica phases is a left lateral shift in the apex position from 22.2° 2θ or 4.00 Å (opal-A) to 21.75° 2θ or 4.09 Å (opal-A/CT, opal-CT, opal-C) to 20.85° 2θ or 4.26 Å (quartz).

3.5. Scanning electron microscopy (SEM)

Fresh (hydrated) to lightly silicified microbial mat samples were investigated with a Philips (FEI) SEM XL30S field emission gun at the Research Centre for Surface and Materials Science (UOA) using two preparation and analytical methods—(1) fixed and critical-point dried samples that were then imaged using steps also applied to solid sinter samples (below) and (2) frozen/sublimated samples analyzed on a Gatan 2500 Cryo Transfer System attached to the scanning electron microscope. For method (1), fresh microbial mat was collected in the field and placed immediately into vials filled with spring water. Samples were then transferred into a solution of 5% glutaraldehyde. In the laboratory, mat samples were placed in a series of ethanol baths of varying concentrations (10%, 30%, 50%, 70%, 95%, 100%) for at least 30 min. These critical-point dried samples, as well as samples of solid sinter, then were mounted on aluminum stubs and powder-coated with platinum (10 nm coating thickness) for 2–10 min at 10 mA with a high-resolution Polaron SC7640 sputter coater. Operating conditions were an accelerating
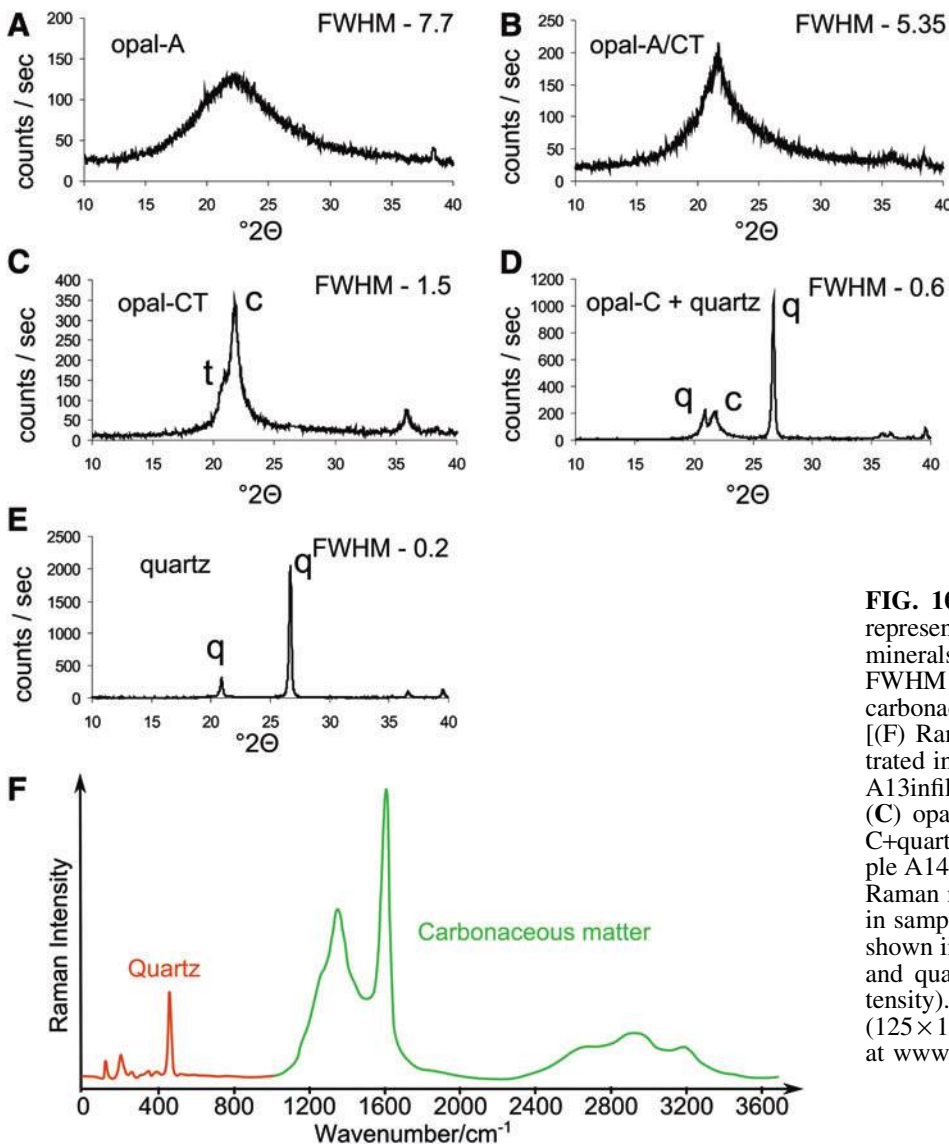
FIG. 10. Sinter compositional data for representative New Zealand silica phase minerals [(A–E) XRPD traces with their FWHM values; Table 2] and Jurassic carbonaceous filaments encased in quartz [(F) Raman spectrum; from sample illustrated in Fig. 9C–9E]. (**A**) opal-A, sample A13infill; (**B**) opal-A/CT, sample A2001; (**C**) opal-CT, sample A4white; (**D**) opal-C+quartz, sample A100; (**E**) quartz, sample A1402white. (**F**) WITec Alpha 500RA Raman map of filamentous palisade fabric in sample C105 with carbonaceous matter shown in green (1600 cm^{-1} peak intensity) and quartz in orange (465 cm^{-1} peak intensity). The scan size is $250 \times 250 \, \mu m^2$ (125×125 px). (Color graphics available at www.liebertonline.com/ast)

voltage of 5–20 keV, a spot size of 3 μm, and a working distance of 10 mm. For method (2), recently collected field samples placed in 50% spring water and 50% ethanol (95%), and stored on ice, were frozen rapidly in a liquid nitrogen slush to minimize ice-crystal formation. Subsequently, structural water was sublimated at −95°C to reveal the intact, three-dimensional mat network. Cryo–scanning electron microscope samples were then cooled to <−135°C and coated with gold-palladium for 120 s under vacuum and imaged at 5 keV accelerating voltage at −180°C.

3.6. Petrography and mineral and carbon mapping of thin sections

Polished thin sections were examined with optical light microscopy and laser micro-Raman spectrometry to calibrate SEM results for New Zealand sinter and to map mineral and carbon distributions in Jurassic sinter. Raman mapping was undertaken on Patagonian sample C105 using a WITec Alpha500 RA system with a green laser ($\lambda = 532$ nm, Nd:YAG

frequency doubled laser) at the Centre de Biophysique Moléculaire, Orléans, France. The laser is connected to the system via an optical fiber and is focused on the surface by optical microscope objectives. A sample scanning system allows mapping over areas ranging from a few square micrometers to up to several square centimeters. The configuration used for this study produced a laser spot size of ~ 850 nm, with laser power set at 5 mW at the surface, at a spectral range of ~ 4000 cm^{-1} and a resolution of ~ 3 cm^{-1}. The compositional maps are made by color scaling the intensity of the main peak of each compound with different colors (*e.g.*, the 465 cm^{-1} peak for the quartz and the 1600 cm^{-1} for the carbonaceous matter). The spatial resolution is given by the ratio of the scan size over the number of pixels.

4. Results

4.1. Overview

The biological composition, siliceous textures, and preservation state of the low-temperature palisade microfacies

undergoing diagenesis (opal-A to quartz) were traced by using the variety of analytical techniques outlined above. Mats and sinter from the TVZ, New Zealand, provided samples with an age span of modern to ~6500 years BP (unpublished data), encompassing the opal-A to quartz silica phase sinter maturation sequence. In addition, a representative, well-preserved sample of Jurassic (~150 Ma) sinter, now quartz, was studied from the Claudia sinter deposit, Deseado Massif, Argentina (Guido and Campbell, 2014).

4.2. Molecular characterization of modern microbial mats

Clone library–based 16S rRNA gene analysis of samples from modern dark brown-green microbial mats, with feltlike palisade textures, revealed that all (KP1–4, KP7, 2KP1, 3OK4; Table 1) were dominated by a shared member of the mesophilic cyanobacterial genus, *Calothrix* (Fig. 7). This prevailing OTU was present in libraries at 34–74% relative abundance and shared 99% sequence identity with *Calothrix* sp. CCMEE5093 (GenBank accession AY147029). Other cyanobacterial sequences variably present across these samples were related to an unclassified subsection III cyanobacterium (Tomitani *et al.*, 2006), *Leptolyngbya*, *Anabaena*, and *Synechococcus* species, and *Calothrix desertica* (93% identity).

In contrast, the dark brown, conical tufted mat sample 3KP2 was dominated by 2 OTUs related to *Oscillatoria* (22% abundance, 98–99% identical to *Oscillatoria* sp. J24Osc, AF263344) and populated by a lower abundance (15%) of *Calothrix*, with minor proportions of *Leptolyngbya*, *Anabaena*, and *Synechococcus* species. Samples OK5 (paler brown/white-brown transition) and 3OK1 (mucilaginous) were microbiologically distinct, as they contained no identifiable *Calothrix* species. OK5 was dominated by *Oscillatoria* and *Leptolyngbya* spp. at 12% and 9% relative abundance, respectively, while 3OK1 was highly enriched in *Leptolyngbya* spp. (90% abundance), in particular a single OTU closely related to *Leptolyngbya* sp. CENA 103 (99% identity, accession EF088339).

The *Chloroflexus* signature identified by lipid analysis of deep mat layers (below) was not captured by DNA-based analysis, likely due to either under-sampling of the deeper layers for molecular analyses, which were restricted to the living, largely unsilicified portion of the mats, or low proportional representation of *Chloroflexus* in homogenized, mixed-layer samples. Chloroflexi was observed in only one microbial mat sample from Orakei Korako where the discharging fluid temperature was 36°C (Table 1, Fig. 7).

4.3. Lipid biomarkers

In the living dark green-brown, feltlike mat sampled from M1 on Golden Fleece Terrace, Orakei Korako, a general decrease in abundance of most lipid biomarkers, particularly phospholipid fatty acids (PLFAs) (indicators of living biomass), was observed from the top to lower layers, that is, L1 to L3 (Fig. 6A, 6C–6F), suggesting decreasing microbial abundances with depth. Typical biomarkers for cyanobacteria, including n-C19 alkane, monomethyl alkanes and alkenes (Shiea *et al.*, 1991), decreased through the depth of the mat (Fig. 8A). In comparison, those indicative of *Chloroflexus* species (green nonsulfur bacteria), such as wax esters and hentriacontatriene (Zeng *et al.*, 1992), increased

in abundance in lower layers (Fig. 8B). *Chloroflexus* is a genus of Gram-negative facultative phototrophs that grow heterotrophically in the light or dark when in the presence of oxygen (Pierson and Castenholz, 1974; Hanada *et al.*, 1995). In addition, algal biomarkers, such as polyunsaturated fatty acids, were most abundant in the uppermost layers.

The top layer (L1, Fig. 6E) was dominated by n-C16 free fatty acid, n-C16 PLFA, and the C_{16} and C_{18} monounsaturated fatty acids and PLFAs (various sources). Other compounds present in high abundance included n-C17 alkane, 17:1 and 18:1 alkenes, and 7-methylheptadecane, biomarkers typical of cyanobacteria. While alkanes also were present in the deeper layers, albeit in lower abundance, the unsaturated hydrocarbons were completely absent beneath L1 (Fig. 8). Phytadienes and phytol (derived from chlorophyll *a* found in cyanobacteria) also were present, but their occurrence was variable. Although the highest abundance of phytadienes was found in L2 (Fig. 6D), no phytol was detected in this layer, suggesting its degradation. Taken together, the summed abundances of phytol and the phytadienes showed little change through the mat (L1–L4), and in lower layers may have represented remnants of a past cyanobacterial community. Moreover, diploptene, a bacterial biomarker with a pentacyclic triterpenoid structure, showed increasing abundance with depth in the mat. The source of this compound is unclear. Hentriacontatriene and wax esters, typical of *Chloroflexus*, were observed in deeper layers, in concentrations much lower than those observed for cyanobacterial biomarkers. Since *Chloroflexus* can act as a heterotroph in the absence of light, the higher abundance of this biomarker signature at greater depth would be expected, assuming oxygen availability, which was likely owing to the close proximity of oxygenic cyanobacteria in the upper mat layers.

In siliceous layer four (L4, Fig. 6F), lipid biomarker concentrations were about 2 orders of magnitude lower than those observed in the overlying mat. Unsaturated hydrocarbons and highly unsaturated fatty acids appear to have been poorly preserved and were not detected in the sinter (Fig. 8). This basal silica deposit underlying the living mat was dominated by n-C16 free fatty acid, n-C16 PLFA, and 18:1 PLFA, all of which can be derived from a wide range of sources and, thus, lack diagnostic information. Several compounds found in the L4 sinter, such as numerous wax esters, bishomohopanol, and branched fatty acids, were absent in the overlying mat layers (L1–L3). Some compounds may represent degradation products (*e.g.*, bishomohopanol may derive from hopanoids); nonetheless, at the time of sinter formation, a different microbial assemblage to that observed in the overlying mat layers may have been present.

For comparison, lipid biomarkers were extracted from Rainbow Terrace (site M2) from a dark green to brown living mat forming distal sinter-apron terracettes (Fig. 6B). A similar biomarker distribution to the L4 sample on Golden Fleece Terrace was observed, that is, a dominance of n-C16 and n-C18 free fatty acids, and n-C16 and n-C18 PLFAs. Moreover, unsaturated hydrocarbons and highly unsaturated fatty acids, most likely derived from the overlying microbial mat, also were present. The most dominant compounds were n-C16 free fatty acid, 18:1 fatty acid, n-C16 PLFA, and n-C18 PLFA (various sources). Methyl diploptene (cyanobacterial biomarker; Summons *et al.*, 1999) also was present in relatively high abundance. Other bacterial biomarkers included unsaturated hydrocarbons and monomethyl alkanes (found in

cyanobacteria), β-OH fatty acids (typically found in Gram-negative bacteria), and branched free fatty acids and PLFAs. Phytol and phytadiene, degradation products of chlorophyll a found in cyanobacteria, also were present. It is evident that the M2 mat is predominantly cyanobacterial; however, the occurrence of 18:3 fatty acid also suggests an algal input.

From the biomarker abundances, it is clear that very little was preserved in the relict sinter (A5) sampled from Golden Fleece Terrace, Orakei Korako (Fig. 5C). Only n-C17 alkane, n-C19 alkane, and diploptene were identified in the neutral fraction, present at abundances at least an order of magnitude lower than the fresh sinter associated with the living mats shown in Fig. 6. The most abundant compounds in the A5 relict sinter sample were n-C16 and n-C18 free fatty acids, which have many sources and lack specificity. Surprisingly, PLFAs, which typically only last a few days after cell death, also were present in sample A5, hinting that silicification may, in some cases, facilitate biogeochemical preservation. Other biomarkers preserved in sample A5 included branched free fatty acids and PLFAs (*iso* and *anteiso* C17), which are typically found in bacteria.

Attempts to extract specific biomarkers from Jurassic sinter in Patagonia have thus far returned a result of unspecified hydrocarbons (n-alkanes, isoprenoids, hopanes; R. Pancost, personal communication, 2013) and are under further investigation.

4.4. Silica phase minerals and silicification of palisade fabric

Forty-seven horizons of TVZ palisade fabric were analyzed by XRPD to determine the silica phase present within each horizon. Samples revealed a range of silica phase minerals from opal-A to quartz (Table 2; Fig. 10). The modern (fresh) sample from Rainbow Terrace at Orakei Korako was the most mineralogically immature, opal-A sinter, with a FWHM value of $8.05°$ 2θ. Ancient deposits from Orakei Korako consisted of opal-A (FWHM values $7.7–6.7°$ 2θ) and opal-CT (FWHM values $\sim 0.8°$ 2θ). Samples from Sinter Island produced a range of silica phases from opal-A (FWHM value of $6.4°$ 2θ) to opal A/CT (FWHM value of $5.4°$ 2θ) to opal-CT (FWHM values between 1.5 and $2.5°$ 2θ) and opal-C+quartz (FWHM values between 1.5 and $0.7°$ 2θ). Umukuri samples were the most mature mineralogically, with samples consisting of either opal-C+quartz (FWHM values between 0.8 and $0.5°$ 2θ) or quartz (FWHM value of $0.2°$ 2θ). Twenty-five horizons within 10 samples were analyzed for moganite (following methods in Rodgers and Cressey, 2001), with a trace amount detected in some samples consisting of opal-CT, opal-C, or quartz mineral phases (Table 2).

Initially, where silica entombed the coarse filaments, and during early silica phase maturation (opal-A), the palisade microfacies occurred as distinctive horizons of porous, friable sinter with opaline microspheres adhering to surfaces (Figs. 2, 3). Subsequent mineralogical maturation resulted in void infill, with filaments encrusted and engulfed by a solidifying silica deposit (Figs. 11–13). Silica infill within individual palisade horizons was not uniform, resulting in spatially patchy areas of both well-defined and poorly-defined palisade fabric (Fig. 11B–11F).

4.5. Diagenetic progression in palisade textural characteristics

4.5.1. Modern mats and incipient sinter formation. Two samples of living mat (M1, M2) were collected and examined to identify micron-scale textures and silica mineral morphology and to determine the preservation state of biosignatures within actively depositing sinter upon viable microbial mats of the palisade facies. Samples were collected from the Golden Fleece (sample M1; Fig. 6A, 6C) and Rainbow terraces (sample M2; Fig. 6B), Orakei Korako. At the time of sampling, the water discharging over the Golden Fleece Terrace had a temperature of $31.3°C$ and a pH of 7. The Golden Fleece sample was divided into four layers for analysis (L1–L4; Fig. 6D–6F). Each layer was examined for lipid biomarker preservation (Fig. 8) and to identify any change in textural characteristics with vertical zonation over a depth of 5 mm. Figure 6D shows the various layers analyzed. The uppermost three layers constituted the microbial mat, labeled L1 to L3, with L1 representing the uppermost and youngest layer at the air/water interface. The fourth layer (L4) consisted of newly deposited sinter that was forming immediately underneath the living mat. Sample M2 from Rainbow Terrace constituted a living, low-temperature mat overlying newly deposited sinter. At the time of sampling, water flowing over this mat was $34.5°C$ with a pH of 9 (Fig. 6B).

Petrographic thin section photomicrographs of modern palisade fabric (site M1), within sinter from Golden Fleece Terrace, reveal laminae (up to 1 mm thick) of closely packed, subvertically oriented, silica-encrusted, cyanobacterial sheaths, forming a distinctive palisade sinter microfabric (Fig. 2A–2B). These horizons alternated with laminae of dark porous, fenestral sinter (Fig. 2B). The tightly packed palisade horizon shown in Fig. 2B contained empty filamentous microfossil sheaths (15 μm diameter), with individual erect filaments clearly distinguishable. These filaments were so tightly packed that no silica matrix was visible in thin section. Some horizons were less densely packed (Fig. 2C, 2D), where many of the filaments showed thin, outer sheaths and a dark, grainy, silica infill (Fig. 2C). The amount of silica infill within individual filaments varied from partial to almost complete. In these horizons the matrix consisted of two textures (Fig. 2C, 2D): (1) grainy, translucent silica dominating in zones of few filaments and (2) mottled, dark grainy silica, which was most abundant between filaments in filament-rich horizons.

Scanning electron microscope images of the actively silicifying, modern palisade mat from the Golden Fleece Terrace (site M1) confirmed petrographic observations, showing that this modern mat constituted alternating horizons (150 μm thick) of silica-encrusted filaments and smooth silica horizons (Fig. 3A, 3B). Sharp boundary contacts between the filamentous and smooth silica horizons suggest abrupt transitions in environmental conditions. When conditions were favorable for the establishment of filamentous microbes, communities were well developed, as evidenced by the numerous, closely packed, erect filaments shown in Fig. 2A–2C. When conditions became unsuitable for low-temperature filamentous cyanobacteria to thrive, possibly in relation to changes in flow rates, horizons of smooth silica formed (Fig. 3A, 3B). Individual filaments within the modern mat were in the initial stages of silicification, shown by opal-A spheres (0.5 μm diameter) attached to individual filaments. The filaments were only partially coated in opal-A; in places, they
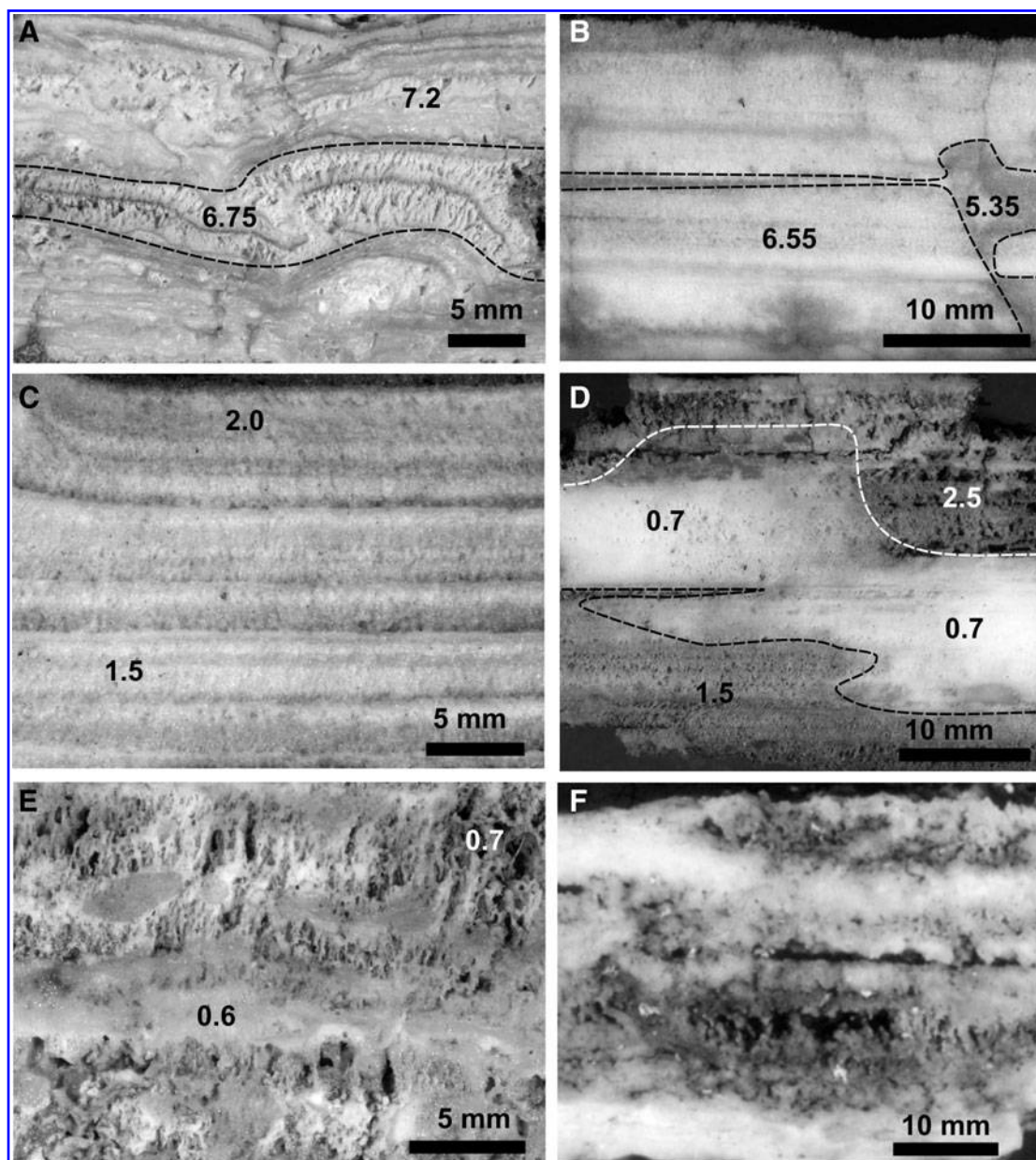
FIG. 11. Representative hand specimen photographs of TVZ palisade fabric throughout the various silica mineral phases encountered during diagenetic from opal-A to quartz. (**A**) Well-defined, opal-A palisade horizon (cross section through a small terracette, as indicated by the rounded step in the laminae) with FWHM value of 6.75° 2θ, enclosed in opal-A with FWHM value of 7.2° 2θ. Sample A18. (**B**) Multiple, thin horizons of opal-A/CT palisade fabric with FWHM values between 5.3 (undergoing patchy diagenetic modification) and 6.6° 2θ. Sample A20. (**C**) Numerous horizons of palisade fabric of opal-CT with FWHM values between 1.5 and 2.0° 2θ. Sample A4. (**D**) Opal-CT horizons showing massive, mottled, diffusely layered fabric, with patchy replacement (white) of originally more porous palisade fabric (FWHM value of 2.5–0.7° 2θ). Sample A22. (**E**) Palisade fabric with opal-C+quartz mineralogy (FWHM values of 0.7–0.6° 2θ). Sample A10. (**F**) Palisade fabric with quartz mineralogy and FWHM value of 0.2° 2θ. From Umukuri sinter.

coalesced to form sphere masses (Fig. 3D). Filaments uncoated with silica revealed exterior sheath diameters of up to 8 μm, while those encrusted with silica had exterior sheath diameters of 10 μm or more (Fig. 3C).

Cross-sectional views of living palisade mat fabrics, preserved by fixation upon sampling and visualized by cryo-SEM techniques, revealed sheathed filaments embedded in smooth to meshlike exopolysaccharide (Fig. 4A). Exterior sheaths and internal trichomes are evident (Fig. 4B), with the initial stages

of silicification indicated by opal-A spheres (0.4 μm diameter) forming around sheath exteriors (Figs. 3D, 4C).

4.5.2. Opal-A and opal-A/CT samples. Mineralogically immature opal-A and opal-A/CT sinter samples of the palisade fabric entombed near vertically oriented, filamentous microbes in a porous, silica matrix (Figs. 11A, 11B, 12A–12C). The microbes forming the palisade textures revealed total exterior diameters of <10 μm and were silicified with
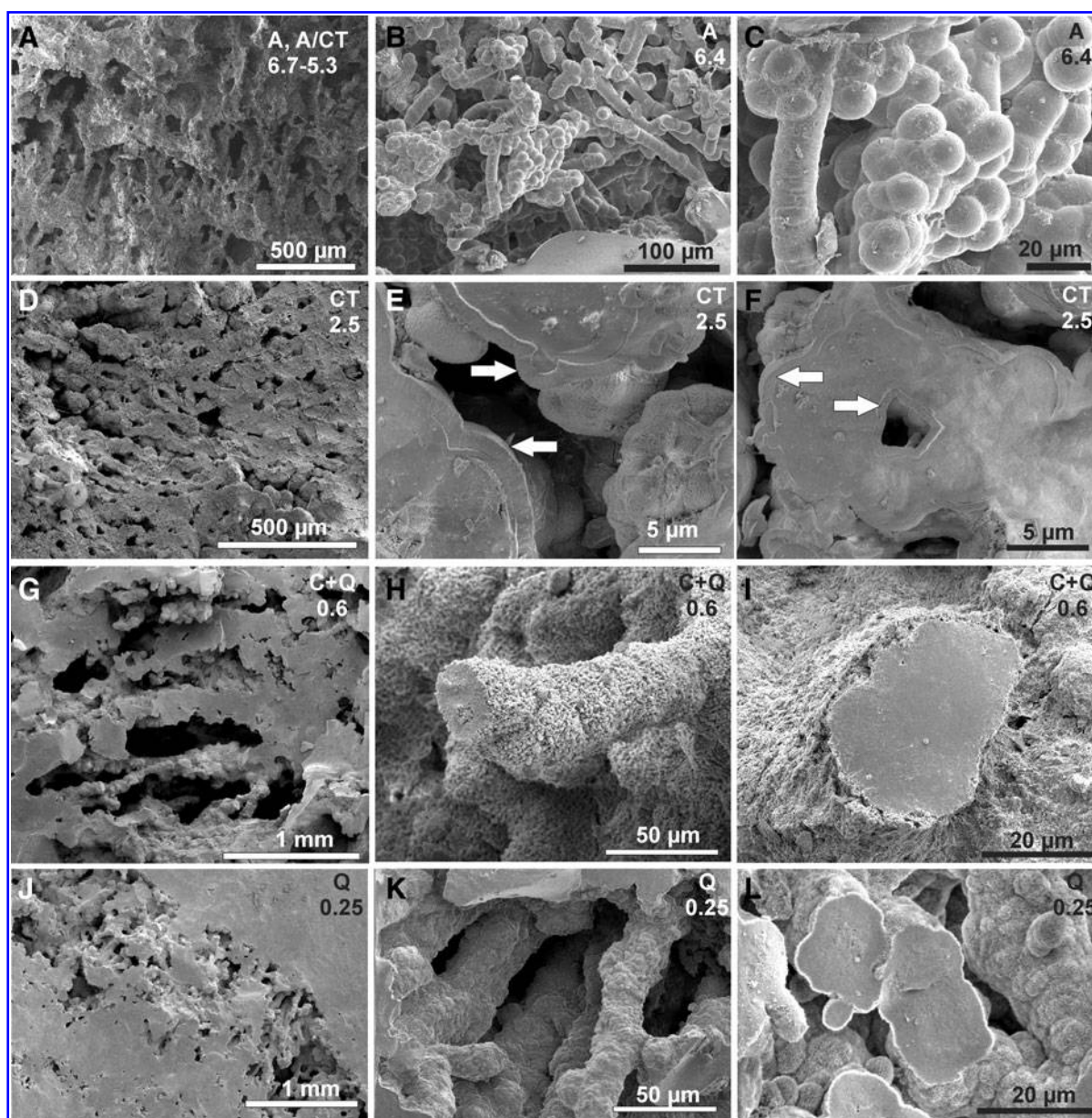
FIG. 12. Scanning electron microscope images of fossil sinter in the TVZ reveal morphology of palisade fabric throughout the various silica mineral phase changes. Letters and numbers shown in upper right corner of each image indicate silica phase and FWHM value in °2θ (A, opal-A; A/CT, opal-A/CT; CT, opal-CT; C, opal-C; Q, quartz). (**A**) Sample A20. (**B–C**) Sample A21. (**D–F**) Sample A22. (**G–I**) Sample A9. (**J–L**) Sample A14.

opal-A spheres (Fig. 11A–11C). Petrographic examination of these horizons revealed hollow tubular molds in a grainy, translucent matrix (Fig. 13A–13C).

4.5.3. Opal-CT samples.

Opal-CT sinter samples of the palisade microfacies (Fig. 11C) constituted horizons of tightly packed, filamentous microbes, with either empty voids between individual filaments or voids containing filament clusters (Figs. 12D, 13D, 13E). Filament exterior diameters (up to 15 μm) increased owing to mineralization of outer sheath surfaces. Opal-CT rims formed around sheath exteriors (Figs. 12E, 12F, 13F) and partially infilled each tubular mold (Figs. 12E, 12F, 13D–13F).

4.5.4. Opal-C and quartz samples.

Within the studied samples, macrotextures remained recognizable for the palisade facies undergoing late-stage diagenesis to opal-C and quartz (Fig. 11E, 11F). In this diagenetic state, voids remained between many of the mineralized filaments, although patchy infill of open spaces with silica did occur in places (Figs. 12E, 12F, 13G, 13J). With maturation to opal-C and quartz, initially hollow tubular molds commonly became completely infilled, such that distinction between filament sheath and mold became difficult if not impossible to detect (Figs. 12I, 12L, 13G–13L). Mineralization of the exterior sheath increased overall filament diameters to >20 μm (Fig. 12H, 12K).
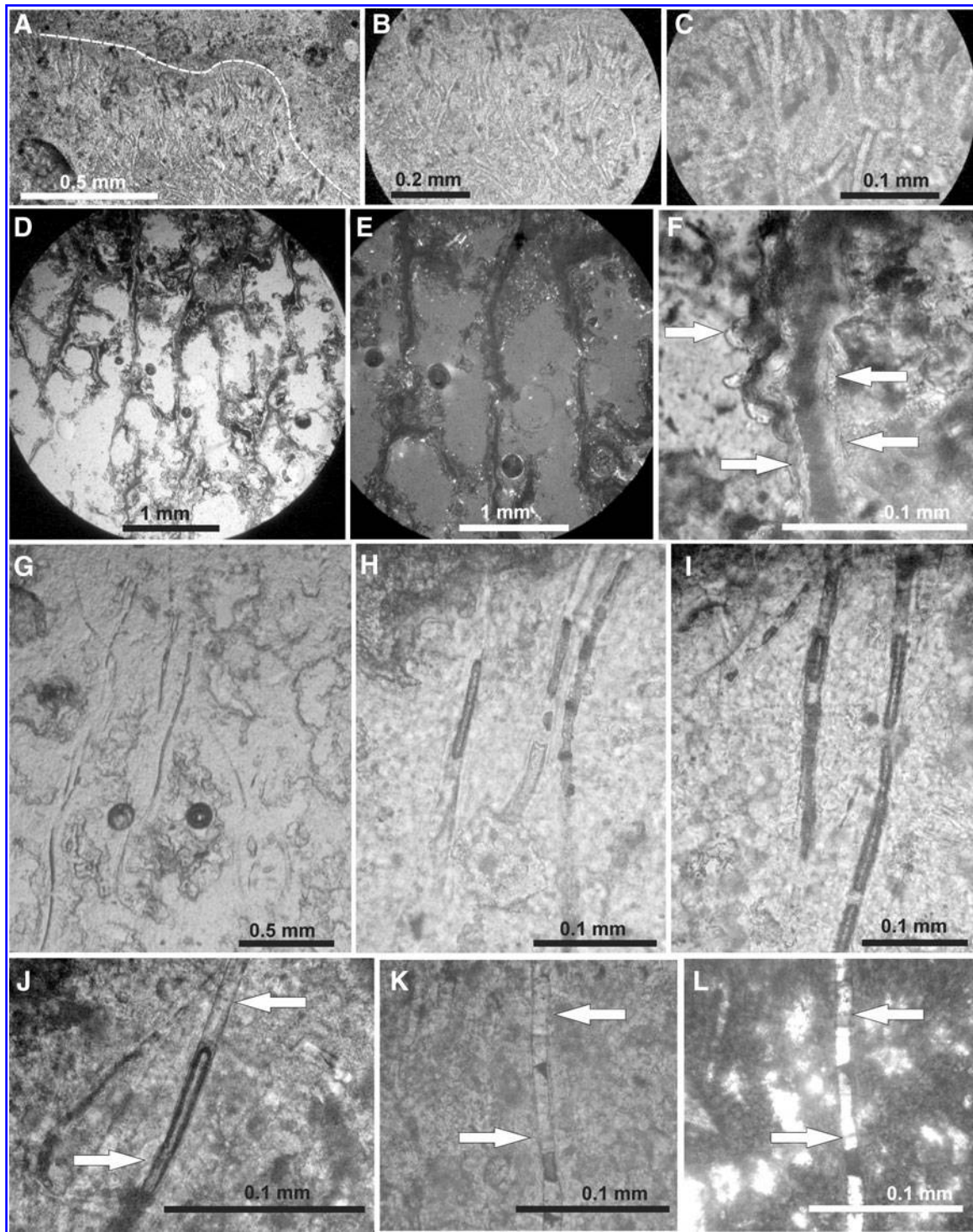
FIG. 13. Thin section photomicrographs of TVZ sinter matrix and inclusions in palisade fabric with opal-A, opal-CT, and opal-C+quartz silica phases. (**A–C**) Opal-A palisade fabric. FWHM value = 7.0–6.5° 2θ. Sample OK79. (A) Overview of opal-A palisade fabric. (B) Vertically oriented filaments within palisade fabric. (C) Increased magnification reveals closely packed filaments with hollow tubular molds. (**D–F**) Opal-CT palisade fabric. FWHM value = 2.0° 2θ. Sample A4. (D) Overview of porous palisade fabric. (E) Detail of (D), in crossed polarized light view, shows patchy recrystallization (bright) within the matrix. (F) View of single filament reveals infill of dark grainy silica, and mineralization increasing on the exterior sheath (arrows). (**G–I**) Opal-C+quartz palisade fabric. FWHM value = 0.8–0.6° 2θ. Sample A9. (G) Overview of filamentous horizon shows preserved palisade filaments in a quartzose matrix. (H–I) Increased magnification reveals filament infill consists of alternating light and dark granular silica. (**J–L**) Opal-C+quartz palisade fabric. FWHM value = 0.7–0.6° 2θ. Sample A10. (J–K) Arrows indicate patchy recrystallization of the granular infill of individual filaments. (L) Crossed-polarized light view of (K) showing patchy recrystallization of the matrix to quartz (white), and the quartzose nature of granular infill.

4.5.5. Late Jurassic filamentous sinter sample from Patagonia. A sinter sample (C105) bearing palisades texture from the Late Jurassic Claudia sinter, Deseado Massif, Argentina (Guido and Campbell, 2014), is an example of excellent preservation of probable photosynthesizing cyanobacterial fossils embedded in a ~150 Ma low-temperature hot-spring deposit (Fig. 9C–9E; Guido and Campbell, 2014). A laser micro-Raman map (Fig. 9E) and Raman spectrum (Fig. 10F) allowed correlation of the filamentous fabric with carbon distribution, encased in quartz. The quartz shows faint microbanding, possibly related to fluctuations in environmental conditions affecting sinter-lamina deposition, or it may be a diagenetic effect. The C105 sample field site is positioned at the intersection of two lineaments, inferred as faults (Fig. 9B); therefore, fluid flow and hence silicification at this site was likely direct, rapid, and/or long-lived, facilitating biosignature preservation (Guido and Campbell, 2014).

5. Discussion

5.1. Molecular biosignatures of microbial mats in New Zealand hot springs

Phylogenetic analysis of brown to dark green, felted, palisade fabric–producing, modern microbial mats from Orakei Korako and Kuirau Park (TVZ), growing in fluids of 29–39°C, revealed a dominance by members of the cyanobacteria, especially those from the genus *Calothrix* (order Nostocales, Fig. 7). This is consistent with lipid biomarker findings from the topmost layer of an analogous mat at Orakei Korako (Fig. 8), indicating a light-exposed, photosynthesizing, mesophilic microbial community. It has been shown elsewhere that *Calothrix* species grow optimally at moderate to low temperatures in geothermal settings and have a reported upper temperature limit of ~48°C (Castenholz, 2015). While many members of the genus have been isolated from, or identified within, marine and brackish settings (Stewart, 1962; Sihvonen *et al.*, 2007), they also are found in freshwater habitats and are commonly identified in tepid thermal spring outflow waters through cultivation or cell morphological characteristics (*e.g.*, Wickstrom and Castenholz, 1978; Hugo *et al.*, 2011).

The vertical distribution of palisade mat inhabitants at Orakei Korako is reflected in the changing distribution of the observed lipids. Cyanobacteria are the dominant species in the uppermost layer of the mat, with algae present in lower abundance. On descending the mat, cyanobacterial biomarkers decrease, and *Chloroflexus* biomarkers are observed. Thus, it is likely that in this mat cyanobacteria act as the main primary producers, indirectly supplying reduced organic compounds to underlying *Chloroflexus* and sustaining their heterotrophic metabolism in a ''canopy'' of ecological interactions that are not preserved in the sinter rock archive. Previous lipid biomarker studies from the TVZ have characterized the archaeal and bacterial lipid biomarker compositions of higher-temperature geothermal springs (68–98°C) than those in this study and thus are not directly comparable owing to strikingly different microbial assemblages (Gibson *et al.*, 2008; Kaur *et al.*, 2008, 2011a, 2011b; Gibson *et al.*, 2014). However, the bacteriohopanepolyol studies did indicate a cyanobacterial component in these high-temperature systems.

Analyses here demonstrated that *Calothrix* dominance may be constrained to certain mat textural types in tepid hot-spring waters, such as felted mats, and their distributions may be influenced by lateral temperature fluctuations of hot-spring discharges. For example, sample 3KP2 from Kuirau Park, Rotorua (Table 1), was observed in the field to be a brown, ''*Calothrix*-like'' microbial mat growing over conical tufted fabrics that normally are found in thermal fluids of somewhat higher temperatures of mid-sinter apron settings, suggesting a cooling trend at this location overprinting earlier, warmer facies. Molecular results showed a dominance of *Oscillatoria* rather than *Calothrix* in this ''mixed'' textural and phylogenetic assemblage. Indeed, over >15 years of visiting the Kuirau Park and Orakei Korako sites, we have observed significant and frequent shifting of brown-colored (dominantly *Calothrix*) versus orange to green (dominantly *Oscillatoria*/*Leptolyngbya*) mat surface distributions in the outflow channels, owing to seasonality or channel switching-derived differences in temperature, and changes in discharge rate. Furthermore, in the Lower Geyser Basin of Yellowstone National Park (USA), Schubotz *et al.* (2013) studied microbial diversity in hot springs using lipid biomarkers and 16S rRNA to also find shifting and flexible metabolisms and community diversity in streamer biofilms, driven by changes in environmental conditions (*e.g.*, organic inputs). Also at Yellowstone, Havig *et al.* (2011) documented large variations in carbon and nitrogen values of thermophilic microbes as a function of downstream sampling of hot-spring discharge channels along a temperature gradient, thereby illustrating significant shifts in ecological functions, and hence community compositions, with decrease in temperature. Ecological shifts also occur with depth owing to physicochemical changes in mat ''canopies'' within the mat-sediment system (Schopf and Klein, 1992; Jones *et al.*, 1997a), which also affects community composition and potentially the preservation state of buried, mineralizing mat horizons. For example, heterotrophs within sediments could modify phototrophic filamentous mats entering the burial realm, and we have observed degradation of buried *Calothrix* directly beneath living mat horizons (*e.g.*, Fig. 14C showing poorly preserved old palisade fabric underlying a fresh palisade horizon). Given the large amount of variation in environmental conditions experienced by living mat communities and biofilms growing in geothermal systems, and their subsequent burial and diagenesis, it is remarkable that the main biofacies characteristics of vent-to-marsh settings (Farmer, 2000), that is, taphonomically durable sheathed cyanobacteria, plants, insects, are robust and identifiable over at least 400 million years of the geological record (*e.g.*, Trewin, 1993, 1996; Walter *et al.*, 1996; Guido and Campbell, 2011).

5.2. Controls on preservation potential and fossil quality in sinters

Hot-spring deposits in the Deseado Massif, TVZ, and in other parts of the world, are typically positioned along faults where fluids migrate(d) along permeable pathways to the surface. Where affiliated with cross-faults and/or epithermal veins, geothermal systems may exhibit especially good fossil preservation because of their close spatial relationship
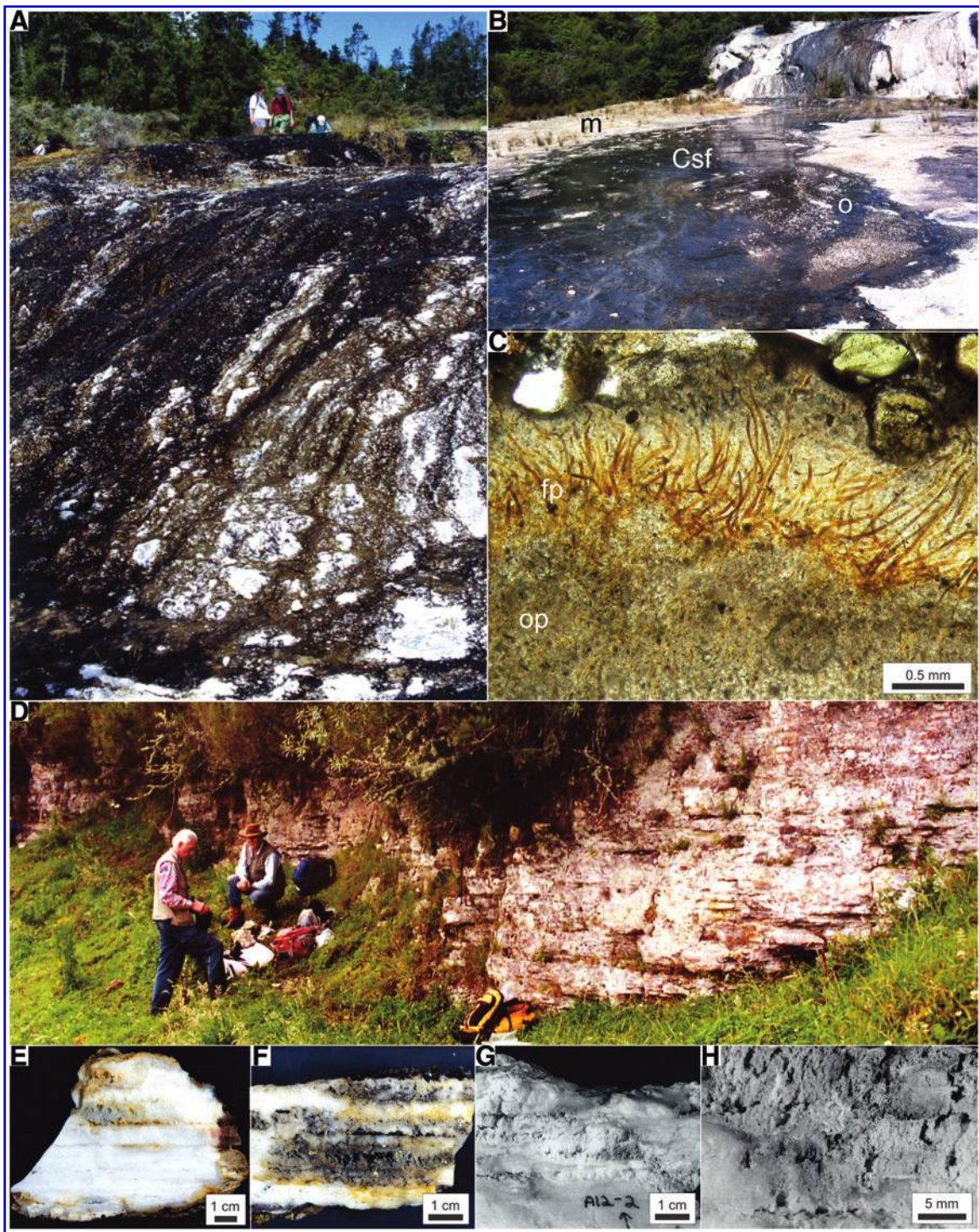
FIG. 14. Preservation potential of robust signatures of microbial palisade fabric into the geological record. (**A**) A period of wet, tepid (<40°C), thermal spring sheet flow over fault-bound, Golden Fleece Terrace, Orakei Korako, TVZ, New Zealand. Site M1 from which samples were collected for biomarker analysis. (**B**) Conditions favoring optimal depositional conditions for palisades facies development—extended, slow, continuous shallow sheet flow of low-temperature geothermal fluids over Golden Fleece Terrace fostering luxuriant growth of dark brown to green *Calothrix* mats. The *Calothrix* sheet flow (Csf) is spilling into and covering adjacent facies areas, in this case flooding oncoid (o) patches and a geothermal marsh (m). (**C**) Young sinter (~60 years old) from Healy's Bore 2 sinter apron at Tokaanu, TVZ, showing a fresh, silicified, filamentous palisade horizon with preserved orange pigment (fp) overlying an older, brown, degraded, silicified palisade horizon (op). Hot-spring activity ceased when an event washed detrital volcanic clasts over the sinter apron. (**D**) Field view of Holocene fossil Umukuri sinter, showing laminated to bedded, largely palisade facies undergoing patchy recrystallization to quartz (whiter areas of outcrop; Campbell *et al.*, 2001). (**E–H**) Hand sample views of palisade fabric from Umukuri, which are partially replaced by massive, mottled, quartzose patches (*cf.* Walter *et al.*, 1996) that have obliterated fine textural details of microbial influence. (Color graphics available at www.liebertonline.com/ast)

with long-lived fluid conduits tapping deep reservoirs and transporting dissolved minerals to Earth's surface along crustal zones of weakness (*e.g.*, Guido and Campbell, 2011, 2012, 2014; Drake *et al.*, 2014). Low-temperature hot-spring facies, that is, distal sinter aprons and geothermal wetland settings, appear to contain the best preservation along the vent-to-marsh environmental gradient, with both early and rapid silicification the key to formation of exceptional fossils (*e.g.*, Trewin, 1993, 1996; Cady and Farmer, 1996; Trewin *et al.*, 2003; Engel and Grimaldi, 2004; Guido *et al.*, 2010; Channing *et al.*, 2011; García Massini *et al.*, 2012; Channing and Edwards, 2013). In particular, such exceptional preservation ideally manifests in permanently wet, cool ($\sim$20–30°C), low-energy, geothermally influenced ponds and marshy areas undergoing silica deposition under slightly reducing conditions (Trewin *et al.*, 2003; Guido *et al.*, 2010).

Calothrix is commonly observed in geothermal settings (*e.g.*, Walter, 1976; Cady and Farmer, 1996; Pentecost, 2005; Lynne, 2012). This photosynthetic cyanobacterium thrives in shallow, low-temperature (<40°C), thermal discharge that slowly spreads out across distal-apron areas (Figs. 6, 14A, 14B). Upon silicification of the dark green to brown, felted microbial mats, a distinctive palisade sinter texture accumulates that constitutes alternating porous/filament-rich and solid/filament-poor horizons, which are typically stacked vertically in $\sim$0.5–1 cm thick layers (*e.g.*, Figs. 1A, 3, 11, 14C). This depositional stacking is likely controlled by a "pulse-pause" style of sheet flow, which may shift from continuous, to gradually or abruptly declining, or to locally ceasing altogether owing to channel switching, climatic conditions, or episodic dormancy of a spring vent. If the necessary conditions for survival of *Calothrix* are not met, a change in sinter texture may be observed. For example, pulsed flow may increase relative silicification rate and produce solid sinter horizons with scattered filaments, while very shallow, quiet ponding in terracettes may enhance vertical growth of densely packed, microbial pillars. Therefore, the thickness, extent, and quality of preserved palisade textures may indicate relative stability or fluctuation of sinter-apron paleoenvironmental conditions, as well as signal the intensity of postdepositional modifications affecting a given location (Fig. 14). Scanning electron microscope images of newly silicified *Calothrix* mats from Orakei Korako (Fig. 3) indicate that the thermal discharge bathing this area behaves in a pulse-pause manner. Repeated site visits over >15 years to the M1 locality, where a newly silicified mat was collected for this study (Figs. 6, 14A), indicate that this area undergoes shifting conditions over several years, from laterally extensive apron-terrace discharge overflowing into adjacent facies types (*e.g.*, Fig. 14B, showing *Calothrix* invading oncoid and plant-dominated marsh areas during a wet cycle) to intervals when the terrace surface is completely dry.

Previous work by Lynne and Campbell (2003, 2004) examined diagenetic change in sinter, specifically during the silica mineral phase transformation from amorphous opal to microcrystalline quartz. This study extends their analyses to include detailed molecular characterization of the living microbes that build the palisades fabric and focuses on the preservation potential of this widespread hot-spring facies over a greater time span (Recent to Late Jurassic). Many studies have noted that the taphonomically robust, polysaccharide sheaths of cyanobacteria readily silicify and rapidly build up mid- to distal-apron sinter deposits (*e.g.*, Walter, 1976; Cady and Farmer, 1996; Mountain *et al.*, 2003; Lynne, 2012). Molecular characterization of such mats herein indicates that the dominant taxa indeed are also the most durable and fossilizable in this accreting portion of the hot-spring system. However, there are also numerous examples where biotic preservation is quite poor, even within local patches of the same fossil hydrothermal system, such as within outcrops of the Holocene Umukuri (Fig. 14D–14H), Pleistocene Artist Point, Jurassic La Marciana, and Devonian Drummond Basin sinters (Walter *et al.*, 1996; Campbell *et al.*, 2001; Hinman and Walter, 2005; Guido and Campbell, 2009). Massive, mottled, diffusely layered fabrics are often all that remains of palisade textures that have undergone strong, secondary silica infill of primary porosity and intense diagenesis (*e.g.*, Fig. 14E–14H; Walter *et al.*, 1996; Campbell *et al.*, 2001; Hinman and Walter, 2005). Age appears to have little to no relation to fossil quality, but rather environmental (*e.g.*, early silicification vs. corrosion by steam acid sulfate condensate) and postdepositional events (*e.g.*, tectonic transition to passive margin vs. continued explosive volcanism) may fortuitously align to provide windows on exceptional fossil preservation in paleo-hydrothermal systems.

6. Conclusions

In summary, the mesothermophilic genus *Calothrix* is a common and dominant, mat-forming, photosynthesizing cyanobacterium that produces a distinctive palisade fabric in silica-bearing, tepid thermal spring discharge areas globally. Its robust, thick polysaccharide sheaths create a taphonomic bias toward preferential preservation, while other components of the complex microbial community within and beneath the surface mat horizon, confirmed by molecular analyses, are largely lost upon passage into the geological record. Distal siliceous sinter aprons accumulate thick sequences of palisade fabrics, and the originally porous deposits typically undergo patchy diagenetic recrystallization in the mineralogical transformation from opal to quartz. In some cases of combined rapid and early mineralization, followed by minimal postdepositional disturbance, fossil preservation quality may be exceptional. Fortuitous local environmental conditions and the regional geological history of each deposit dictate the overall quality of fossil preservation in the deep-time sinter archive.

References

Altschul, S.F., Gish, W., Miller, W., Myers, E.W., and Lipman, D.J. (1990) Basic local alignment search tool. *J Mol Biol* 215:403–410.

Bignall, G. (1991) Subsurface stratigraphy and structure of the Orakei Korako and Te Kopia geothermal systems. In *Proceedings of the 13th Geothermal Workshop*, Auckland University, Auckland, pp 199–206.

Bignall, G. (1994) Thermal evolution and fluid-rock interactions in the Orakeikorako-Te Kopia geothermal system, Taupo Volcanic Zone, New Zealand. PhD thesis (unpublished), University of Auckland, Auckland.

Bock, G.R. and Goode, J.A., editors. (1996) *Evolution of Hydrothermal Ecosystems on Earth (and Mars?)*, Ciba Foundation Symposium 202, Wiley and Sons, Chichester, UK.

Cady, S.L. and Farmer, J.D. (1996) Fossilization processes in siliceous thermal springs: trends in preservation along thermal gradients. In *Evolution of Hydrothermal Ecosystems on Earth (and Mars?)*, Ciba Foundation Symposium 202, edited by G.R. Bock and J.A. Goode, John Wiley and Sons, Chichester, UK, pp 150–173.

Campbell, K.A. and Lynne, B.Y. (2006) Diagenesis and dissolution at Sinter Island (456 yrs BP), Taupo Volcanic Zone: silica stars and the birth of quartz. In *Proceedings of the 28th New Zealand Geothermal Workshop*, Auckland.

Campbell, K.A., Sannazzaro, K., Rodgers, K.A., Herdianita, N.R., and Browne, P.R.L. (2001) Sedimentary facies and mineralogy of the Late Pleistocene Umukuri silica sinter, Taupo Volcanic Zone, New Zealand. *Journal of Sedimentary Research* 71:727–746.

Campbell, K.A., Buddle, T.F., and Browne, P.R.L. (2003) Late Pleistocene silica sinter associated with fluvial, lacustrine, volcaniclastic and landslide deposits at Tahunaatara, Taupo Volcanic Zone, New Zealand. *Trans R Soc Edinb Earth Sci* 94:485–501.

Campbell, K.A., Guido, D.M., Gautret, P., Foucher, F., Ramboz, C., and Westall, F. (2015) Geyserite in siliceous hot-spring sinter: window on Earth's hottest terrestrial (paleo) environment and its extreme life. *Earth-Science Reviews* 148:44–64.

Cassie, V. (1989) A taxonomic guide to thermally associated algae (excluding diatoms) in New Zealand. *Bibliotheca Phycologica* 78:1–159.

Castenholz, R.W. (2015) Portrait of a geothermal spring, Hunter's Hot Springs, Oregon. *Life* 5:332–347.

Channing, A. and Edwards, D. (2013) Wetland megabias: ecological and ecophysiological filtering dominates the fossil record of hot spring floras. *Palaeontology* 56:523–556.

Channing, A., Edwards, D., and Guido, D. (2011) *Equisetum thermale* sp. nov. (Equisetales) from the Jurassic San Agustín hot spring deposit, Patagonia: anatomy, paleoecology and inferred paleoecophysiology. *Am J Bot* 98:680–697.

Drake, B.D., Campbell, K.A., Rowland, J.V., Guido, D.M., Browne, P.R.L., and Rae, A. (2014) Evolution of a dynamic paleo-hydrothermal system at Mangatete, Taupo Volcanic Zone, New Zealand. *Journal of Volcanology and Geothermal Research* 282:19–35.

Engel, M.S. and Grimaldi, D.A. (2004) New light shed on the oldest insect. *Nature* 427:627–630.

Eriksson, K.A. and Truswell, J.F. (1974) Tidal flat associations from a Lower Proterozoic carbonate sequence in South Africa. *Sedimentology* 21:293–309.

Farmer, J.D. (2000) Hydrothermal systems: doorways to early biosphere evolution. *GSA Today* 10:1–9.

Farmer, J.D. and Des Marais, D.J. (1994) Biological versus inorganic processes in stromatolite morphogenesis: observations from mineralizing sedimentary systems. In *Microbial Mats: Structure, Development and Environmental Significance*, edited by L.J. Stal and P. Caumette, NATO Advanced Science Institute, Series G35, Springer-Verlag, Berlin, pp 61–68.

Farmer, J.D. and Des Marais, D. (1999) Exploring for a record of ancient martian life. *J Geophys Res* 104:26977–26995.

Fayers, S.R. and Trewin, N.H. (2003) A review of the palaeoenvironments and biota of the Windyfield chert. *Trans R Soc Edinb Earth Sci* 94:325–339.

Flörke, O.W., Graetsch, H., Martin, K., Roller, K., and Wirth, R. (1991) Nomenclature of micro- and non-crystalline silica minerals, based on structure and microstructure. *Neues Jahrbuch für Mineralogie Abhandlungen* 163:19–42.

Fournier, R.O. (1985) The behaviour of silica in hydrothermal solutions. *Reviews in Economic Geology* 2:45–62.

Fournier, R.O. and Rowe, J.J. (1966) Estimation of underground temperatures from the silica content of water from hot springs and steam wells. *Am J Sci* 264:685–697.

García Massini, J., Channing, A., Guido, D.M., and Zamuner, A.B. (2012) First report of fungi and fungus-like organisms from Mesozoic hot springs. *Palaios* 27:55–62.

Gibson, R.A., Talbot, H.M., Kaur, G., Pancost, R.D., and Mountain, B.W. (2008) Bacteriohopanepolyol signatures of cyanobacterial and methanotrophic bacterial populations recorded in a geothermal vent sinter. *Org Geochem* 39:1020–1023.

Gibson, R.A., Sherry, A., Kaur, G., Pancost, R.D., and Talbot, H.M. (2014) Bacteriohopanepolyols preserved in silica sinters from Champagne Pool (New Zealand) indicate a declining temperature gradient over the lifetime of the vent. *Org Geochem* 69:61–69.

Graetsch, H. (1994) Structural characteristics of opaline and microcrystalline silica minerals. *Reviews in Mineralogy* 29:209–232.

Guido, D.M. and Campbell, K.A. (2009) Jurassic hot-spring activity in a fluvial setting at La Marciana, Patagonia, Argentina. *Geological Magazine* 146:617–622.

Guido, D.M. and Campbell, K.A. (2011) Jurassic hot spring deposits of the Deseado Massif (Patagonia, Argentina): characteristics and controls on regional distribution. *Journal of Volcanology and Geothermal Research* 203:35–47.

Guido, D.M. and Campbell, K.A. (2012) Diverse subaerial and sublacustrine hot spring settings of the Cerro Negro epithermal system (Jurassic, Deseado Massif), Patagonia, Argentina. *Journal of Volcanology and Geothermal Research* 229–230:1–12.

Guido, D.M. and Campbell, K.A. (2014) A large and complete Jurassic geothermal field at Claudia, Deseado Massif, Santa Cruz, Argentina. *Journal of Volcanology and Geothermal Research* 275:61–70.

Guido, D.M., Channing, A., Campbell, K.A., and Zamuner, A. (2010) Jurassic geothermal landscapes and fossil ecosystems at San Agustín, Patagonia, Argentina. *J Geol Soc London* 167:11–20.

Guidry, S.A. and Chafetz, H.S. (2002) Factors governing subaqueous siliceous sinter precipitation in hot springs: examples

from Yellowstone National Park, U.S.A. *Sedimentology* 49: 1253–1267.

Guidry, S.A. and Chafetz, H.S. (2003a) Depositional facies and diagenetic alteration in a relict siliceous hot spring accumulation: examples from Yellowstone National Park, U.S.A. *Journal of Sedimentary Research* 73:806–823.

Guidry, S.A. and Chafetz, H.S. (2003b) Siliceous shrubs in hot springs from Yellowstone National Park, Wyoming, U.S.A. *Can J Earth Sci* 40:1571–1583.

Guidry, S.A. and Chafetz, H.S. (2003c) Anatomy of siliceous hot-springs: examples from Yellowstone National Park, Wyoming, U.S.A. *Sediment Geol* 157:71–106.

Hamlin, K.A. (1999) Geological studies of the Orakei Korako geothermal field, Taupo Volcanic Zone. MSc thesis (unpublished), University of Auckland, Auckland.

Hanada, S., Hiraishi, A., Shimada, K., and Matsuura, K. (1995) *Chloroflexus aggregans* sp. nov., a filamentous phototrophic bacterium which forms dense cell aggregates by active gliding movement. *Int J Syst Bacteriol* 45:676–681.

Handley, K.M. and Campbell, K.A. (2011) Character, analysis and preservation of biogenicity in terrestrial siliceous stromatolites from geothermal settings. In *Stromatolites: Interaction of Microbes with Sediments*, Cellular Origin, Life in Extreme Habitats and Astrobiology Vol. 18, edited by V.C. Tewari and J. Seckbach, Springer, Dordrecht, pp 359–381.

Handley, K.M., Turner, S., Campbell, K.A., and Mountain, B. (2008) Silicifying biofilm exopolymers on a hot spring microstromatolite: templating nanometer-thick laminae. *Astrobiology* 8:747–770.

Havig, J.R., Raymond, J., Meyer-Dombard, D.R., Zolotova, N., and Shock, E.L. (2011) Merging isotopes and community genomics in a siliceous sinter-depositing hot spring. *J Geophys Res* 116, doi:10.129/2010JG001415.

Herdianita, N.R., Browne, P.R.L., Rodgers, K.A., and Campbell, K.A. (2000a) Mineralogical and textural changes accompanying ageing of silica sinter. *Mineralium Deposita* 35: 48–62.

Herdianita, N.R., Rodgers, K.A., and Browne, P.R.L. (2000b) Routine instrumental procedures to characterise the mineralogy of modern and ancient silica sinters. *Geothermics* 29:65–81.

Hinman, N.W. and Walter, M.R. (2005) Textural preservation in siliceous hot spring deposits during early diagenesis: examples from Yellowstone National Park and Nevada, U.S.A. *Journal of Sedimentary Research* 75:200–215.

Hochstetter, F. von. (1864) *Geology of New Zealand: Contributions to the Geology of the Provinces of Auckland and Nelson*, translated by C.A. Fleming, Government Printer, Wellington, 1959, pp 1–320.

Hofmann, A. and Harris, C. (2008) Silica alteration zones in the Barberton Greenstone Belt: a window into subseafloor processes 3.5–3.3 Ga ago. *Chem Geol* 257:221–239.

Hugo, R.C., Cady, S.L., and Smythe, W. (2011) The role of extracellular *Calothrix:* evidence from microbial mat communities in hot springs at Yellowstone National Park, USA. *Geomicrobiol J* 28:667–675.

Jones, B. and Renaut, R.W. (2007) Microstructural changes accompanying the opal-A to opal-CT transition; new evidence from the siliceous sinters of Geysir, Haukadalur, Iceland. *Sedimentology* 54:921–948.

Jones, B. and Segnit, E.R. (1971) The nature of opal I: nomenclature and constituent phases. *Journal of the Geological Society of Australia* 18:57–68.

Jones, B., Renaut, R.W., and Rosen, M.R. (1997a) Vertical zonation of biota in microstromatolites associated with hot springs, North Island, New Zealand. *Palaios* 12:220–236.

Jones, B., Renaut, R.W., and Rosen, M.R. (1997b) Biogenicity of silica precipitation around geysers and hot-spring vents, North Island, New Zealand. *Journal of Sedimentary Research* 67:88–104.

Jones, B., Renaut, R.W., and Rosen, M.R. (1998) Microbial biofacies in hot-spring sinters: a model based on Ohaaki Pool, North Island, New Zealand. *Journal of Sedimentary Research* 68:413–434.

Jones, B., Renaut, R.W., and Rosen, M.R. (2001) Taphonomy of silicified filamentous microbes—implications for identification. *Palaios* 16:580–592.

Jones, K. (1992) Diurnal nitrogen fixation in tropical *Lyngbya* sp. and heterocystous *Calothrix* sp. *British Phycological Journal* 27:107–118.

Jordan, S. (2007) Microbial communities of two New Zealand hydrothermal systems. PhD thesis (unpublished), The University of Auckland, Auckland.

Kaur, G., Mountain, B.W., and Pancost, R.D. (2008) Microbial membrane lipids in active and inactive sinters from Champagne Pool, New Zealand: elucidating past geothermal chemistry and microbiology. *Org Geochem* 39:1024–1028.

Kaur, G., Mountain, B.W., Hopmans, E.C., and Pancost, R.D. (2011a) Preservation of microbial lipids in geothermal sinters. *Astrobiology* 11:259–274.

Kaur, G., Mountain, B.W., Schouten, S., and Pancost, R.D. (2011b) Relationship between lipid distribution and geochemical environment within Champagne Pool, Waiotapu, New Zealand. *Org Geochem* 42:1203–1215.

Knoll, A.H. (1985) Exceptional preservation of photosynthetic organisms in silicified carbonates and silicified peats. *Philos Trans R Soc Lond B Biol Sci* 311:111–122.

Konhauser, K.O., Jones, B., Reysenbach, A.-L., and Renaut, R.W. (2003) Hot spring sinters: keys to understanding Earth's earliest life forms. *Can J Earth Sci* 4:1713–1724.

Lloyd, E.F. (1972) Geology and hot springs of Orakei Korako. *New Zealand Geological Survey Bulletin* 85:1–164.

Lowe, D.R., Anderson, K.S., and Braustein, D. (2001) The zonation and structuring of siliceous sinter around hot springs, Yellowstone National Park, and the role of thermophilic bacteria in its deposition. In *Thermophiles: Biodiversity, Ecology and Evolution*, edited by A.L. Reysenbach, M. Voytek, and R. Mancinelli, Kluwer Academic/Plenum Publishers, New York, pp 143–166.

Lynne, B.Y. (2012) Mapping vent to distal-apron hot spring paleo-flow pathways using siliceous sinter architecture. *Geothermics* 43:3–24.

Lynne, B.Y. and Campbell, K.A. (2003) Diagenetic transformations (opal-A to quartz) of low- and mid-temperature microbial textures in siliceous hot-spring deposits, Taupo Volcanic Zone, New Zealand. *Can J Earth Sci* 40:1679–1696.

Lynne, B.Y. and Campbell, K.A. (2004) Morphologic and mineralogic transitions from opal-A to opal-CT in low-temperature siliceous sinter diagenesis, Taupo Volcanic Zone, New Zealand. *Journal of Sedimentary Research* 74: 561–579.

Lynne, B.Y., Campbell, K.A., Moore, J., and Browne, P.R.L. (2005) Diagenesis of 1900-year-old siliceous sinter (opal-A to quartz) at Opal Mound, Roosevelt Hot Springs, Utah, U.S.A. *Sedimentary Geology* 119:249–278.

Lynne, B.Y., Campbell, K.A., James, B., Browne, P.R.L., and Moore, J.N. (2007) Tracking crystallinity in siliceous hot-spring deposits. *Am J Sci* 307:612–641.

Maliva, R.G., Knoll, A.H., and Simonson, B.M. (2005) Secular change in the Precambrian silica cycle: insights from chert petrology. *GSA Bulletin* 117:835–845.

Miller, D.N., Bryant, J.E., Madsen, E.L., and Ghiorse, W.C. (1999) Evaluation and optimization of DNA extraction and purification procedures for soil and sediment samples. *Appl Environ Microbiol* 65:4715–4724.

Mountain, B.W., Benning, L.G., and Boerema, J.A. (2003) Experimental studies on New Zealand hot spring sinters: rates of growth and textural development. *Can J Earth Sci* 40: 1643–1667.

Pankhurst, R., Riley, T., Fanning, C.Y., and Kelley, S. (2000) Episodic silicic volcanism in Patagonia and the Antarctic Peninsula: chronology of magmatism associated with the break-up of Gondwana. *Journal of Petrology* 41:605–625.

Pentecost, A. (2005) *Travertine*, Springer, Berlin.

Pierson, B.K. and Castenholz, R.W. (1974) A phototrophic gliding filamentous bacterium of hot springs, *Chloroflexus aurantiacus*, gen. and sp. nov. *Arch Microbiol* 100:5–24.

Renaut, R.W. and Jones, B. (2011) Hydrothermal environments, terrestrial. In *Encyclopedia of Geobiology*, edited by J. Reitner and V. Thiel, Springer, Dordrecht, pp 467–479.

Renaut, R.W., Jones, B., and Rosen, M.R. (1996) Primary silica oncoids from Orakeikorako hot springs, North Island, New Zealand. *Palaios* 11:446–458.

Richardson, N.J. and Underhill, J.R. (2002) Controls on the structural architecture and sedimentary character of syn-rift sequences, North Faulkland Basin, South Atlantic. *Mar Pet Geol* 19:417–443.

Riley, T., Leat, P., Pankhurst, R., and Harris, C. (2001) Origin of large volume rhyolitic volcanism in Antarctic Peninsula and Patagonia by crustal melting. *Journal of Petrology* 42: 1043–1065.

Rodgers, K.A. and Cressey, G. (2001) The occurrence, detection and significance of moganite (SiO_2) among some silica sinters. *Mineral Mag* 65:157–167.

Ruff, S.W., Farmer, J.D., Calvin, W.M., Herkenhoff, K.E., Johnson, J.R., Morris, R.V., Rice, M.S., Arvidson, R.E., Bell, J.F., III, Christensen, P.R., and Squyres, S.W. (2011) Characteristics, distribution, origin and significance of opaline silica observed by Spirit rover in Gusev Crater, Mars. *J Geophys Res* 116, doi:10.1029/2010JE003767.

Saul, D.J., Aislabie, J.M., Brown, C.E., Harris, L., and Foght, J.M. (2005) Hydrocarbon contamination changes the bacterial diversity of soil from around Scott Base, Antarctica. *FEMS Microbiol Ecol* 53:141–155.

Schalamuk, I., Rubia, M., Genini, A., and Fernández, R. (1997) Jurassic epithermal Au-Ag deposits of Patagonia, Argentina. *Ore Geology Reviews* 12:173–186.

Schopf, J.W. and Klein, C., editors. (1992) *The Proterozoic Biosphere: A Multidisciplinary Study*, Cambridge University Press, Cambridge, UK.

Schubotz, F., Meyer-Dombard, D.R., Bradley, A.S., Fredricks, H.F., Hinrichs, K.-U., Shock, E.L., and Summons, R.E. (2013) Spatial and temporal variability of biomarkers and microbial diversity reveal metabolic and community flexibility in streamer biofilm communities in the Lower Geyser Basin, Yellowstone National Park. *Geobiology* 11, doi:10.1111/GBI.12051.

Sheppard, D.S. and Lyon, G.L. (1984) Geothermal fluid chemistry of the Orakeikorako field, New Zealand. *Journal of Volcanology and Geothermal Research* 22:329–349.

Shiea, J., Brassell, S.C., and Ward, D.M. (1991) Comparative analysis of extractable lipids in hot spring microbial mats and their component photosynthetic bacteria. *Org Geochem* 17: 309–319.

Sihvonen, L.M., Lyra, C., Fewer, D.P., Rajaniemi-Wacklin, P., Lehtimäki, J.M., Wahlsten, M., and Sivonen, K. (2007) Strains of the cyanobacterial genera *Calothrix* and *Rivularia* isolated from the Baltic Sea display cryptic diversity and are distantly related to *Gloeotrichia* and *Tolypothrix*. *FEMS Microbiol Ecol* 61:74–84.

Simmons, S.F. and Browne, P.R.L. (1991) *Active Geothermal Systems of the North Island, New Zealand*, Geological Society of New Zealand Miscellaneous Publication 57, Geological Society of New Zealand, Wellington.

Smith, D.K. (1998) Opal, cristobalite, and tridymite: non-crystallinity versus crystallinity, nomenclature of the silica minerals and bibliography. *Powder Diffr* 13:2–19.

Steiner, A. (1977) The Wairakei geothermal area North Island, New Zealand. *New Zealand Geological Survey Bulletin* 90: 1–136.

Stetter, K.O. (1996) Hyperthermophilic prokaryotes. *FEMS Microbiol Rev* 18:149–158.

Stewart, W.D.P. (1962) Fixation of elemental nitrogen by marine blue-green algae. *Ann Bot* 26:439–445.

Summons, R.E., Jahnke, L.J., Hope, J.M., and Logan, G.A. (1999) 2-Methylhopanoids as biomarkers for cyanobacterial oxygenic photosynthesis. *Nature* 400:554–557.

Tomitani, A., Knoll, A.H., Cavanaugh, C.M., and Ohno, T. (2006) The evolutionary diversification of cyanobacteria: molecular–phylogenetic and paleontological perspectives. *Proc Natl Acad Sci USA* 103:5442–5447.

Trewin, N.H. (1993) Depositional environment and preservation of biota in the Lower Devonian hot-springs of Aberdeenshire, Scotland. *Trans R Soc Edinb Earth Sci* 84:433–442.

Trewin, N.H. (1996) The Rhynie chert: an early Devonian ecosystem preserved by hydrothermal activity. In *Evolution of Hydrothermal Ecosystems on Earth (and Mars?)*, Ciba Foundation Symposium 202, edited by G.R. Bock and J.A. Goode, John Wiley and Sons, Chichester, UK, pp 131–149.

Trewin, N.H., Fayers, S.R., and Kelman, R. (2003) Subaqueous silicification of the contents of small ponds in an Early Devonian hot-spring complex, Rhynie, Scotland. *Can J Earth Sci* 40:1697–1712.

Walter, M.R. (1976) Hot-springs sediments in Yellowstone National Park. In *Stromatolites*, Developments in Sedimentology 20, edited by M.R. Walter, Elsevier, Amsterdam, pp 489–498.

Walter, M.R., Des Marais, D., Farmer, J.D., and Hinman, N.W. (1996) Lithofacies and biofacies of mid-Paleozoic thermal spring deposits in the Drummond Basin, Queensland, Australia. *Palaios* 11:497–518.

Walter, M.R., McLoughlin, S., Drinnan, A.N., and Farmer, J.D. (1998) Paleontology of Devonian thermal spring deposits, Drummond Basin, Australia. *Alcheringa* 22:285–314.

Watanabe, M.M. and Kurogi, M. (1975) Taxonomic *Calothrix scopulorum* and *C. crustacea*. *Botanical Magazine-Tokyo* 88:111–125.

Weed, W.H. (1889) On the formation of siliceous sinter by the vegetation of thermal springs. *Am J Sci* 37:351–359.

Weres, O. and Apps, J.A. (1982) Prediction of chemical problems in the reinjection of geothermal brines. In *Recent Trends in Hydrogeology*, edited by T.N. Marasimhan, Geological Society of America Special Paper 189, Geological Society of America, Boulder, CO, pp 407–426.

Westall, F., de Wit, M.J., Dann, J., van der Gasst, S., de Ronde, C.E.J., and Gerneke, D. (2001) Early Archean fossil bacteria and biofilms in hydrothermally influenced sediments from the Barberton greenstone belt, South Africa. *Precambrian Res* 106:93–116.

Westall, F., Campbell, K.A., Bréhéret, J.-G., Foucher, F., Gautret, P., Hubert, A., Soreiul, S., Grassineau, N., and Guido, D.M. (2015) Archean (3.33 Ga) microbe-sediment systems were diverse and flourished in a hydrothermal context. *Geology* 43:615–618.

Wickstrom, C.E. and Castenholz, R.W. (1978) Association of *Pleurocapsa* and *Calothrix* (cyanophyta) in a thermal stream. *J Phycol* 14:84–88.

Williams, L.A. and Crerar, D.A. (1985) Silica diagenesis, II. General mechanisms. *Journal of Sedimentary Petrology* 55:312–321.

Zeng, Y.B., Ward, D.M., Brassell, S.C., and Eglinton, G. (1992) Biogeochemistry of hot spring environments: 3. Apolar and polar lipids in the biologically active layers of a cyanobacterial mat. *Chem Geol* 95:347–360.

Address correspondence to:
Kathleen A. Campbell
Earth Science Programme
School of Environment
Private Bag 92019
The University of Auckland
Auckland 1142
New Zealand

E-mail: ka.campbell@auckland.ac.nz

Abbreviations Used

FWHM = full width at half maximum
GC = gas chromatography
GC-MS = gas chromatography–mass spectrometry
OTU = operational taxonomic unit
PLFAs = phospholipid fatty acids
RFLP = restriction fragment length polymorphism
SEM = scanning electron microscopy
TVZ = Taupo Volcanic Zone
UOA = University of Auckland
XRPD = X-ray powder diffraction